

FUNCTIONAL AND STRUCTURAL STUDIES OF MITOCHONDRIAL PORIN

**(c) Copyright by Gregory S. Runke
August 2000**

A thesis submitted in partial fulfilment of the requirements for the degree of

Master of Science

**Department of Microbiology
University of Manitoba
Winnipeg, Manitoba**



National Library
of Canada

Acquisitions and
Bibliographic Services

395 Wellington Street
Ottawa ON K1A 0N4
Canada

Bibliothèque nationale
du Canada

Acquisitions et
services bibliographiques

395, rue Wellington
Ottawa ON K1A 0N4
Canada

Your file Votre référence

Our file Notre référence

The author has granted a non-exclusive licence allowing the National Library of Canada to reproduce, loan, distribute or sell copies of this thesis in microform, paper or electronic formats.

The author retains ownership of the copyright in this thesis. Neither the thesis nor substantial extracts from it may be printed or otherwise reproduced without the author's permission.

L'auteur a accordé une licence non exclusive permettant à la Bibliothèque nationale du Canada de reproduire, prêter, distribuer ou vendre des copies de cette thèse sous la forme de microfiche/film, de reproduction sur papier ou sur format électronique.

L'auteur conserve la propriété du droit d'auteur qui protège cette thèse. Ni la thèse ni des extraits substantiels de celle-ci ne doivent être imprimés ou autrement reproduits sans son autorisation.

0-612-53217-8

Canada

THE UNIVERSITY OF MANITOBA
FACULTY OF GRADUATE STUDIES

COPYRIGHT PERMISSION PAGE

Functional and Structural Studies of Mitochondrial Porin

BY

Gregory S. Runke

**A Thesis/Practicum submitted to the Faculty of Graduate Studies of The University
of Manitoba in partial fulfillment of the requirements of the degree
of
Master of Science**

GREGORY S. RUNKE © 2000

Permission has been granted to the Library of The University of Manitoba to lend or sell copies of this thesis/practicum, to the National Library of Canada to microfilm this thesis/practicum and to lend or sell copies of the film, and to Dissertations Abstracts International to publish an abstract of this thesis/practicum.

The author reserves other publication rights, and neither this thesis/practicum nor extensive extracts from it may be printed or otherwise reproduced without the author's written permission.

Abstract

Mitochondrial porin is a voltage-gated, anion-selective channel that facilitates the diffusion of small hydrophilic molecules across the mitochondrial outer membrane. The "glycine-leucine-lysine" (GLK) motif of porin is highly conserved among different species even though overall sequence similarity is quite low. The GLK motif is thought to be part of the ATP binding site for porin. ATP binding is known to alter ion selectivity of *N. crassa* porin. The GLK motif of *N. crassa* porin was changed to GLE through site-directed mutagenesis. Cross-linking studies with ^{32}P -ATP indicate that the GLE mutant was able to bind ATP while electrophysiological measurements indicate that the GLE mutant is able to form a pore in lipid bilayers with altered ion selectivity. Therefore, the GLK motif may not be part of the ATP binding site or the ATP binding site may involve additional amino acid residues other than the GLK motif. The altered ion selectivity of the GLE mutant supports models indicating that the GLK motif is found in the β -barrel of porin.

Several versions of a β -barrel structural model have been proposed for mitochondrial porin. To further refine these models, a series of mutant versions of the porin of *Neurospora crassa* were generated. Each mutant porin harbours a deletion of five amino-acid residues in the carboxyl-terminal half of the protein. These deletions created porins with one of four types of electrophysiological characteristics in black lipid bilayers. Several of the mutants did not form stable pores, identifying regions critical for pore formation had been removed. Other mutant porins formed relatively small pores with altered or absent voltage-dependent gating potentials. Normal pores were formed by one

deletion version of porin, indicating a region not essential for either gating or pore formation. Taken together, the characteristics of the pores formed by these mutant proteins are compatible with either a 16- or a 14-stranded β -barrel structure for mitochondrial porin.

Acknowledgements

I would especially like to thank Dr. Deborah Court for allowing me to work in her lab. Her support, generosity, patience, help, insight and guidance are all very much appreciated. I would like to thank Dr. Joe O'Neil for sitting on my committee and for all of his support and help with circular dichroism spectroscopy. Thanks to Dr. Elizabeth Worobec for also sitting on my committee and for her help and input into my project. I would also like to acknowledge Darren Manley who helped with the circular dichroism spectroscopy and Jillian Waruk for her contributions towards this project. This research was funded by NSERC and the University of Manitoba Research Grants Program.

Table of Contents

Abstract	i
Acknowledgements	iii
List of Figures	vi
List of Tables	viii
List of Abbreviations	ix
 CHAPTER 1	
1.1. Introduction	1
1.2. Potential extra-mitochondrial locations of mitochondrial porin	2
1.3. Functional properties of mitochondrial porin	2
1.3.1. Electrophysiological properties	2
1.3.2. Functional aspects voltage-dependent gating	2
1.4. Structural properties of mitochondrial porin	4
1.4.1. Information obtained from the analysis of 2-dimensional crystals	5
1.4.2. Structural models of porin	5
1.4.2.1. The 12-stranded β -barrel model	6
1.4.2.2. The 13-stranded β -barrel model	9
1.4.2.3. The Rauch and Moran 16-stranded β -barrel model	10
1.4.2.4. The Popp 16-stranded β -barrel model	13
1.4.2.5. The 19-stranded β -barrel model	13
1.4.3. Structural implications to porin gating	13
1.4.4. Circular dichroism studies of porin	17
1.5. Similarities and differences between the E. coli OmpF porin and mitochondrial porins	18
1.5.1. Sequence similarity	18
1.5.2. Structural properties of OmpF porin	20
1.5.3. Functional comparisons	25
1.6. Objectives	25
 CHAPTER 2	
Materials and Methods	28
2.1. Bacterial strains and plasmids	28
2.2. Plasmid DNA isolation	28
2.3. DNA manipulation	28
2.3.1. Site-directed mutagenesis	28
2.3.2. General cloning methods	31
2.4. Protein expression and purification	33

2.5. Sodium dodecylsulfate-polyacrylamide gel electrophoresis	34
2.6. Western immunoblotting of $\Delta 163$ -166 porin	34
2.7. Preparation of porin proteins for biochemical and biophysical analysis	35
2.8. Concentrating of protein on Centricon columns	35
2.9. Cross-linking of purified His ₆ porin and GLEporin to [³² P]-ATP through periodate oxidation	36
2.10. Lipid bilayer experiments	36
2.11. Circular dichroism	37
CHAPTER 3	
GLEporin Mutant Results and Discussion	38
3.1. Site-directed mutagenesis	38
3.2. Cloning of the GLEporin mutant into pQE-9	41
3.3. GLEporin expression, purification and dialysis	44
3.4. ATP binding by GLEporin	44
3.5. Single channel properties of GLEporin	49
3.6. Circular dichroism studies	54
3.7. Discussion	58
3.7.1. Single channel conductance, voltage gating and ion selectivity of the GLE mutant	58
3.7.2. Interactions of GLEporin with ATP	59
3.7.3. Circular Dichroism	60
CHAPTER 4	
Functional Characterization of Porin Mutants	62
4.1. Deletion mutagenesis and cloning into pQE-9	62
4.2. Deletion mutant expression, purification and dialysis	63
4.3. Single channel properties	68
4.3.1. Single channel conductance	68
4.3.2. Voltage-dependent gating	73
4.4. Discussion	82
4.4.1. Characterization of deletion mutants	82
4.4.2. Implications to structural models of porin	88
4.4.2.1. Model 1	88
4.4.2.2. Model 2	97
4.5. Summary	102
4.6. Future Work	102
References	104

List of Figures

Fig. 1.1. The 12-stranded and 13-stranded β -barrel models of mitochondrial porin	7
Fig. 1.2. The 16-stranded β -barrel models of mitochondrial porin	11
Fig. 1.3. The 19-stranded β -barrel model of mitochondrial porin	14
Fig. 1.4. The three dimensional structure of the <i>E. coli</i> OmpF porin	21
Fig. 3.1. The conserved GLK motif	39
Fig. 3.2. Ethidium bromide stained 2% agarose gel of the <i>Xho</i> I-digested pBluescript SK ⁻ plasmids and restriction map	42
Fig. 3.3. Coomassie Blue stained SDS-PAGE of GLEporins	45
Fig. 3.4. Covalent coupling of [α - ³² P]ATP to His ₆ porin and GLEporin	47
Fig. 3.5. Single channel recording of GLEporin	50
Fig. 3.6. Voltage dependence of His ₆ porin and GLEporin	52
Fig. 3.7. Circular dichroism analyses of His ₆ porin and GLEporin	55
Fig. 4.1. Coomassie Blue stained SDS-PAGE of deletion mutant porins	64
Fig. 4.2. Western blot of Δ 163-166porin and His ₆ porin	66
Fig. 4.3. Histograms of the conductance fluctuations of Δ 148-152porin, Δ 167-171porin, Δ 178-182porin, Δ 187-191porin and wild-type porin	69
Fig. 4.4. Histograms of the conductance fluctuations of Δ 196-200porin, Δ 229-233porin, Δ 238-242porin, Δ 243-248porin and wild-type porin	71
Fig. 4.5. Voltage dependent gating of Δ 148-152porin and Δ 167-171porin	74
Fig. 4.6. Voltage dependent gating of Δ 178-182porin and Δ 187-191porin	76
Fig. 4.7. Voltage dependent gating of Δ 196-200porin and Δ 229-233porin	78
Fig. 4.8. Voltage dependent gating of Δ 238-242porin and Δ 243-248porin	80

Fig. 4.9. The current structural models of <i>N. crassa</i> mitochondrial porin	85
Fig. 4.10. The newly proposed 16-stranded β -barrel model, model 1	89
Fig. 4.11. The newly proposed 14-stranded β -barrel model, model 2	98

List of Tables

Table 1.1. Pairwise comparisons of the sequence similarity between the OmpF, PhoE, <i>N. crassa</i> and <i>S. cerevisiae</i> porins	19
Table 2.1. <i>E. coli</i> strains used in this study	29
Table 2.2. Plasmids and bacteriophage used in this study	30
Table 2.3. The mutagenic oligonucleotides used in this study	32
Table 3.1. Compilation of circular dichroism data obtained from <i>Neurospora</i> porins	57
Table 4.1. Electrophysiological data obtained from mutant porins	83
Table 4.2. Hydropathic values assigned to residues in constructing Kyte and Doolittle plots	87
Table 4.3. Values from the Kyte and Doolittle hydropathic plot of <i>N. crassa</i> mitochondrial porin	91
Table 4.4. Kyte and Doolittle plots of the newly formed segments formed in each of the deletions mutants	94

List of Abbreviations

Å	Angstrom
amp^r	Ampicillin Resistant
ATP	Adenosine Triphosphate
bp	Base Pair
β-OG	β-octoglucoside
CCA	Convex Constraint Algorithm
CD	Circular Dichroism
cam^r	Chloramphenicol Resistant
C-terminus	Carboxy Terminus
DiphPC	Diphytanoyl Phosphatidylcholine
DNA	Deoxyribonucleic Acid
EDTA	Ethylenediamine-Tetraacetic Acid
GLE	Glycine-Leucine-Glutamate
GLK	Glycine-Leucine-Lysine
GTP	Guanine Triphosphate
G_u/G₀	Conductance at Voltage U/Conductance at Voltage 0
HEPES	2-Ethane-Sulfonic Acid
His₆	Hexa-HistidinyI Tag
HVDAC1	Human Voltage-Dependent Anion-Selective Channel 1
IPTG	Isopropylthio-β-D-Galactosidase
kan^r	Kanomycin Resistant
Kb	Kilobase
kDa	Kilodalton
LB	Luria-Bertani
LDAO	Lauryl Dimethylamine Oxide
LPS	Lipopolysaccharide
μCi	Microcurrie
μg	Microgram
mg	Milligram
μl	Microlitre
ml	Millilitre
mM	Millimolar
mV	Millivolt
nm	Nanometer
nS	Nanosiemens
Ni-NTA	Nickel-Nitriloactetic Acid-Agarose
N-terminus	Amino Terminus
OmpF	Outer Matrix Protein F
³²P	Phosphorus 32
PBS	Phosphate Buffered Saline

P_C/P_A	Ratio of Cations to Anions
PCR	Polymerase Chain Reaction
PhoE	Phosphoprotein E
rpm	Revolutions Per Minute
SDS-Page	Sodium Dodecylsulfate-Polyacrylamide Gel Electrophoresis
SIR	Single Isomorphous Replacement
TBS	Tris Buffered Saline
tet^r	Tetracycline Resistant
VDAC	Voltage-Dependent Anion-Selective Channel

CHAPTER 1

1.1. Introduction

Mitochondrial porin, a voltage-dependent anion-selective channel (VDAC), spans the outer membrane of the organelle. The biological function of porin is the transport, across the mitochondrial outer membrane, of small molecules required for reactions that occur in the mitochondrion and the cytosol (Colombini, 1979; Roos *et al.*, 1982; Schein *et al.*, 1976; Zalman *et al.*, 1980). It has also been suggested that porin, which is also a component of the permeability transition pore with cyclophilin-D and the adenine nucleotide translocase (Crompton *et al.*, 1998), might be involved in the translocation of cytochrome *c* from the intermembrane space into the cytosol to activate caspases involved in apoptosis (Shimizu *et al.*, 1999). In humans, a deficiency of mitochondrial porin is thought to be a cause of mitochondriopathy (Huizing *et al.*, 1996) which causes psychomotor retardation and minor dysmorphic features.

Porin was originally isolated and studied from the mitochondria of *Paramecium* (Schein *et al.*, 1976). The DNA sequences encoding mitochondrial porins from a number of species are known at present (Blachly-Dyson *et al.*, 1994; Blachly-Dyson *et al.*, 1993; Bureau *et al.*, 1992; Elkeles *et al.*, 1995; Fischer *et al.*, 1994; Ha *et al.*, 1993; Heins *et al.*, 1994; Kayser *et al.*, 1989; Kleene *et al.*, 1987; Mihara and Sato, 1985; Sampson *et al.*, 1996a; Sampson *et al.*, 1996b; Troll *et al.*, 1992). Even though the overall identity in the derived protein sequences is relatively low, channel properties such as voltage dependence, ion selectivity and single-channel conductance are highly conserved. In addition, the proteins are predicted to possess similar secondary structures, containing

stretches of alternating hydrophobic and hydrophilic amino acids that suggest the formation of amphipathic β -strands (Benz, 1994; Blachly-Dyson *et al.*, 1990; De Pinto *et al.*, 1991). Several structural models for mitochondrial porins predict β -barrel cylinders consisting of either 12, 13, 16 or 19 antiparallel, amphiphilic β -strands (Benz, 1994; De Pinto *et al.*, 1991) like those of the bacterial porins (Cowan *et al.*, 1992).

1.2. Potential extra-mitochondrial locations of mitochondrial porin

There is some evidence which suggests that porin might be found in membranes other than the mitochondrial outer membrane. These potential extra-mitochondrial locations include the sarcoplasmic reticulum of skeletal muscle (Shoshan-Barmatz *et al.*, 1996), the plasma membranes of a rat astrocytic cell line (Guibert *et al.*, 1998), endosomes from rat renal cortex (Reymann *et al.*, 1998), synaptosomes (Moon *et al.*, 1999; Shafir *et al.*, 1998), in caveolae (Bathori *et al.*, 1999) and in the plasma membranes of *Xenopus laevis* oocytes (Steinacker *et al.*, 2000). A recent study has also shown that the murine VDAC-1 gene expresses two different porins which differ in their N-terminus such that one porin has a hydrophobic leader peptide which targets it to the cell membrane while the second porin lacks the leader and inserts in the mitochondrial outer membrane (Buettner *et al.*, 2000). Most of these extra-mitochondrial locations for porin occur in specialized cell types, indicating that the need for porin channels in these cells may not be restricted to the mitochondrial outer membrane.

1.3. Functional properties of mitochondrial porin

1.3.1. Electrophysiological properties

The electrophysiology of mitochondrial porin has been studied by porin purification and reconstitution into artificial planar lipid bilayers. The reconstitution of porin into artificial membranes requires a detergent and sterols (Popp *et al.*, 1995). Sterols seem to be important for channel formation before insertion into membranes.

Mitochondrial porin has been found to insert into artificial membranes as a monomer (Mannella *et al.*, 1992), forming water-filled channels that are slightly anion-selective in their maximal-conductance open states (4.0–4.5 nS in 1M KCl) and cation-selective in the low conductance voltage-induced “closed” states (2.0–2.5 nS) (reviewed in Benz, 1994). Porin, in its open state, has a diameter of 2.4–3.0 nm, while in its closed states, the diameter of the pore is thought to be 1.7–1.9 nm (Colombini *et al.*, 1987). The pore formed by porin is voltage-dependent where the high conductance open states are found at transmembrane potentials around zero mV and the pore reversibly closes to its low conductance state at potentials of ± 20 mV and higher (Colombini, 1979).

1.3.2. Functional aspects of voltage-dependent gating

The functional aspects of porin gating, including regulation of the gating process, have been studied in some detail. Functional studies include the role of voltage-gating in the regulation of metabolite and ATP transport through porin channels and the regulation of voltage-dependent gating by different metabolites.

The regulation of the transport of negatively-charged metabolites like citrate, succinate and phosphate by voltage-dependent gating have been studied with porin in artificial bilayers. It was shown that the flux of negatively-charged metabolites through porin was 10–20 times greater in pores that were exposed to low applied voltage

potentials compared to pores exposed to higher applied potentials (Hodge and Colombini, 1997). This indicates that the transport of anions is much greater in pores that are open compared to pores that are in closed states, reinforcing the fact that porin is anion-selective in its open state. Similar results were found in studies of the transport of ATP, with the flux of ATP through porin channels being six times greater in open channels than in closed channels (Rostovtseva and Colombini, 1997). The opposite effect, to a much smaller extent, has been observed in the flux of cations across porin channels with there being a greater flux in the closed states compared to the open states (Hodge and Colombini, 1997).

It has been shown that the voltage-dependent gating of porin can be regulated by metabolites. It was found that both NADH and NADPH can reduce the voltage-dependence of pore closure (Lee *et al.*, 1996). It was observed that a higher concentration of NADPH was required to induce pore closure due to fewer binding sites for NADPH to porin (Lee *et al.*, 1996). It has been shown that König's polyanion can also induce pore closure in a similar manner (Colombini *et al.*, 1987).

Zizi *et al.* (1998) have shown that voltage-dependence can be altered by ion gradients. They found that the voltage-dependence of porin in 1 M KCl was different than in 0.1 M KCl. They also demonstrated that reversing the salt gradient can result in a reversed shift in the gating process. By shifting the activity of the KCl gradient from 0.6 to 0.06, the voltage required to attain the open state of porin shifted from -20 mV to +20 mV (Zizi *et al.*, 1998). This difference in voltage-dependence was found for other salts as well including NaCl, LiCl, KBr, RbBr, potassium acetate and sodium butyrate.

1.4. Structural properties of mitochondrial porin

The three-dimensional structure of mitochondrial porin is unknown to date due to an inability to obtain crystals to perform X-ray crystallography. Some information has been obtained however from the electron microscopy of two-dimensional crystals of porin, but the crystals were found to be too unstable for X-ray crystallography (Mannella, 1989). Due to a lack of a three-dimensional structure of porin, all structural models of mitochondrial porin are derived from secondary structure predictions.

1.4.1. Information obtained from the analysis of 2-dimensional crystals

Based on the two-dimensional crystals of porin, useful information about the structure of porin was obtained. The crystals obtained were from the outer membrane of *Neurospora crassa* mitochondria treated with phospholipase A₂. It was determined that the diameter of porin's lumen was about 3.8 nm (Mannella *et al.*, 1992). This is consistent with the diameter found by passing the largest nonelectrolyte, polyethylene glycol, through the pore, which gave an estimate of 4 nm (Zalman *et al.*, 1980). Two-dimensional crystal analysis also indicated that the repeating structure in the planar crystals was a group of six closely-packed porin proteins in which each protein was separated by 4.3 nm (Mannella *et al.*, 1992). It was also determined from this analysis that each channel was formed by a single polypeptide indicating that porin is functional as a monomer (Mannella *et al.*, 1992).

Recently, crystals of HVDAC1 have been isolated and studied by electron microscopy (Dolder *et al.*, 1999). The unit cell in the crystals was found to consist of two porin monomers. The best resolution obtained for the crystals was 8.2 Å where it was found that the pore lumen had a diameter of 17-20 Å and that each monomer in the unit

cell was separated by 5 Å (Dolder *et al.*, 1999). The mean molecular diameter of HVDAC1 was found to be 37 Å suggesting that the pore is formed by 12-16 β-strands which are tilted 35° (Dolder *et al.*, 1999).

1.4.2. Structural models of porin

As mentioned earlier, the three dimensional structure of mitochondrial porin has not been determined. There are however, different structural models for porin predicted in the literature. These models suggest that porin forms a β-barrel consisting of either 12, 13, 16 or 19 β-strands. These models were predicted by using a combination of different predictive and experimental methods.

1.4.2.1. The 12-stranded β-barrel model

The 12-stranded β-barrel model of the *Saccharomyces cerevisiae* mitochondrial porin (Fig. 1.1A) was constructed by Blachly-Dyson *et al.* (1989). This model was constructed by using Kyte and Doolittle hydropathy plots (Kyte and Doolittle, 1982) to look for 10-residue stretches with β-patterns of alternating polar/nonpolar residues in the human, *S. cerevisiae* and *Neurospora crassa* amino acid sequences. The analyses of these different sequences revealed a common format of peaks in the β-patterns from each sequence. However, a similar search performed with the same analysis on proteins known to form β-barrels produced patterns which were not consistent with the actual protein structure (Mannella *et al.*, 1992). Based on the *S. cerevisiae* sequence analysis, it was determined that there are 12 major peaks in the β-pattern which represented 12 β-strands. Previous studies on the first 20 amino acids of the *Neurospora* sequence revealed that

Fig. 1.1. (A) The 12-stranded β -barrel model of *S. cerevisiae* mitochondrial porin (Blachly-Dyson *et al.*, 1989). The boxes indicate residues which were altered by site-directed mutagenesis that showed a change in ion selectivity while circled residues showed no change in ion selectivity. **(B)** The 13-stranded β -barrel model of *N. crassa* mitochondrial porin (Song *et al.*, 1998b) The numbered residues were changed to cysteine residues and biotinylated. Dashed lines indicate the membrane. The cytosol is at the top of each model.

these residues are able to form an amphiphilic α -helix (Kleene *et al.*, 1987). This led to the formation of a model suggesting that porin is formed by a barrel consisting of 12 β -strands and one α -helix.

The 12-stranded β -barrel model was then tested by constructing a series of point mutations (Fig. 1.1A) designed to alter the net charge in each of the proposed membrane spanning strands and in each of the proposed loops (Blachly-Dyson *et al.*, 1990).

Mutations which caused a change in the ion selectivity and net charge of porin (Fig. 1.1A) indicated residues which are involved in transmembrane regions, while mutations which caused no change (Fig. 1.1A) indicated residues which are not part of a transmembrane region (Blachly-Dyson *et al.*, 1990). Based on these criteria it was found that one β -strand of the original model was misidentified.

1.4.2.2. The 13-stranded β -barrel model

The 13-stranded β -barrel model of the *N. crassa* mitochondrial porin (Fig. 1.1B), which is in part a revision of the *S. cerevisiae* porin 12-stranded β -barrel model, was proposed by Song *et al.* (1998b). The 13-stranded model was constructed based on the results of experiments where single cysteine residues were first introduced into the *N. crassa* porin at two different locations (Song *et al.*, 1998b; Fig. 1.1B). The cysteine residues were then biotinylated in porins isolated from the mitochondrial outer membrane, the porins reconstituted into planar lipid bilayers, and then probed by streptavidin, which is known to bind tightly to biotin (Song *et al.*, 1998b). Streptavidin binding to biotin was found to occur at two different types of sites. Binding at type 1 sites resulted in pores which displayed normal voltage-dependent gating but a reduced single-channel

conductance, while type 2 site binding resulted in pores which were locked in a closed state with no voltage-dependent gating (Song *et al.*, 1998b). It was also found that streptavidin always bound type 1 sites before binding type 2 sites. After determining which cysteine residues acted as type 1 and type 2 sites, constructs with two cysteines were made with one type 1 site and one type 2 site (Song *et al.*, 1998b). Two cysteine residues were determined to be on the same side of the membrane in experiments where streptavidin binding caused a decrease in single-channel conductance and a loss of voltage-dependent gating when added to one side of the membrane while having no effect when added to the opposite side of the membrane (Song *et al.*, 1998b). Conversely, residues were considered to be on opposite sides of the membrane in experiments where the addition of streptavidin to one side of the membrane only caused a decrease in single-channel conductance with no loss of voltage-dependent gating while the addition to the opposite side caused a loss in voltage-dependent gating (Song *et al.*, 1998b). Based on these results, the topology of porin was deduced. This led to the revised 13-stranded β -barrel model with an N-terminal α -helix.

1.4.2.3. The Rauch and Moran 16-stranded β -barrel model

A 16-stranded β -barrel model of the *S. cerevisiae* porin (Fig. 1.2A) was introduced by Rauch and Moran (1994). The model was constructed using a method whereby different porin sequences, both bacterial and mitochondrial, were aligned by their hydrophobic profiles. By applying this model to the different types of porin proteins, it was found that a consensus model of 16 β -strands could be predicted for all mitochondrial porins.

Fig. 1.2. The 16-stranded β -barrel models of **(A)** the *S. cerevisiae* mitochondrial porin (Rauch and Moran, 1994) and **(B)** the *N. crassa* porin (Popp, 1996). Boxed regions indicate predicted transmembrane domains. The shaded areas are not relevant to this discussion.

1.4.2.4. The Popp 16-stranded β -barrel model

Another 16-stranded model was proposed by Popp (1996) for the *N. crassa* mitochondrial porin (Fig. 1.2B). This model was constructed based on results from the analysis of a Kyte and Doolittle hydropathic plot (Kyte and Doolittle, 1982), with some input from protease digestions. The β -strands in this model were predicted to be formed by stretches of alternating hydrophobic/hydrophilic residues from the hydropathic plot. This model also suggests that the N-terminal 20 amino acids are involved in an α -helix located outside of the membrane, which was confirmed by site-directed mutagenesis (Popp *et al.*, 1996).

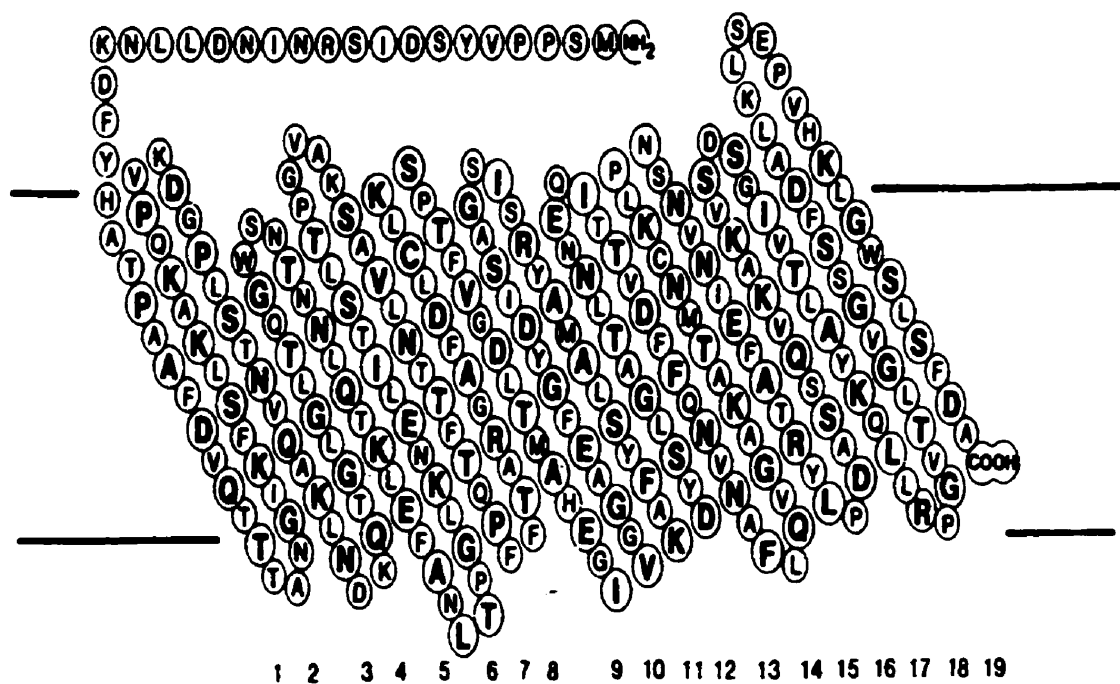
1.4.2.5. The 19-stranded β -barrel model

The 19-stranded β -barrel model of the *S. cerevisiae* mitochondrial porin (Fig. 1.3) was introduced by Forte *et al.* (1987). The model was constructed by using a computer algorithm called the Delphi program (Garnier *et al.*, 1978) which predicts transmembrane segments. In the case of porin, the program was adjusted to favour β -structures and the model produced was of a 19-stranded β -barrel. This model was thought to be valid based on the geometric implications that the β -strands would be tilted 35 degrees with respect to the membrane which would suggest a channel that is 3-3.5 nm in diameter, consistent with what was predicted from two-dimensional crystals (Mannella *et al.*, 1992).

1.4.3. Structural implications to porin gating

The different models for porin structure have been used to predict several mechanisms for gating of porin. The proposal that porin gating might occur by the removal of transmembrane strands from the β -barrel was based on point mutations that

Fig. 1.3. The 19-stranded β -barrel model of the *S. cerevisiae* mitochondrial porin (Forte *et al.*, 1987) which was constructed using the Delphi program.



affect the ion selectivity of both the open and closed states of porin (Peng *et al.*, 1992).

The group which proposed this mechanism was also able to identify potential voltage sensors on porin from the analysis of the voltage-dependence of porin mutants with altered charges (Thomas *et al.*, 1993). If a mutant had an altered voltage-dependence, the residue that was changed in that mutant was considered to be part of the voltage sensor. Residues changed in mutants which had no altered voltage-dependence were not considered to be part of the voltage sensor. They found that lysine, aspartate and glutamate residues acted as voltage sensors (Thomas *et al.*, 1993). There was only a partial relationship between the residues found in the sensor regions and residues which were predicted to be in β -strands that are removed during the gating process. It was concluded that voltage-dependent gating was very complex (Colombini *et al.*, 1996).

An alternative model has also been proposed for the gating mechanism (Mannella, 1997). This model proposes that the gating process occurs through a series of steps. A change in transmembrane potential may trigger the movement of voltage sensors which in turn induces a conformational change to porin (Mannella, 1997). It is proposed that the N-terminal α -helix, which resides in the membrane in porin's open state, may contain the voltage sensors which respond to a stimulus which causes the α -helix to leave the membrane thereby inducing an overall conformational change to porin (Mannella, 1997).

Other authors have argued that the voltage sensors are located within β -strands which form a domain with a net positive charge and that the domain leaves the membrane in response to positive and negative electric field (Song *et al.*, 1998a). This proposed mechanism is based upon the results of the biotin modification experiments which were

used to deduce the 13-stranded β -barrel model.

A model for porin gating based on mechanisms of bacterial porin gating has been proposed by Benz (1994). According to this model, the gate of porin is located in surface exposed loops because the free energy for channel closure is too low between 20 and 40 mV for a β -strand to move from the core of the β -barrel. Based on the model of Popp (1996), two possible candidates for the gate include the loop between β -strands 6 and 7 which is positively charged and the loop between strands 8 and 9 which is neutral. The charged groups within each of these loops could be responsible for the movement of the loops in and out of the pore (Benz, 1994).

1.4.4. Circular dichroism studies of porin

Circular dichroism (CD) studies of *N. crassa* mitochondrial porin were first performed by Shao *et al.* (1996). CD spectra collected in 2% octyl β -glucoside at room temperature and pH 7 indicated that porin has a high β -sheet content (62%). In CD experiments performed at increasing temperatures, it was found that porin had an irreversible loss of β -structure; at 65°C, the β -sheet content was 0% (Shao *et al.*, 1996). The effects of pH on porin structure were also studied and porin was found to have a reversible loss of β -sheet with decreasing pH. At pH 4 and room temperature, porin was found to contain 38% β -sheet in 2% β -OG and porin's structure was fully restored when the pH was returned to 7 (Shao *et al.*, 1996).

The structural properties of *N. crassa* porin with a His₆-containing N-terminal extension has also been studied by CD (Koppel *et al.*, 1998). In spectra of porin, with and without the N-terminal extension, collected in the detergent 1% lauryl dimethylamine

oxide at room temperature and pH 8, it was found that the β -sheet content was unaffected and remained at 45% (Koppel *et al.*, 1998). This result indicated that possessing such N-terminal extensions doesn't change any of the structural properties of the protein detectable by CD.

1.5. Similarities and differences between the *E. coli* OmpF porin and mitochondrial porins

The bacterial porins and mitochondrial porins have certain similarities and differences with respect to their sequences, functional aspects and structures. The three-dimensional structure of the *E. coli* OmpF porin has been solved (Cowan *et al.*, 1992) which has allowed it to be studied in detail with respect to its functional and structural properties. This makes OmpF porin a good representative to use for the bacterial porins in making comparisons to mitochondrial porin.

1.5.1. Sequence similarity

To compare the sequence similarity between bacterial porins and mitochondrial porins, the amino acid sequences of the *E. coli* OmpF and PhoE porins were obtained (Mutoh *et al.*, 1982; Overbeeke *et al.*, 1983) along with the sequences of the *N. crassa* and *S. cerevisiae* porins (Kleene *et al.*, 1987; Mihara and Sato, 1985). The sequence similarity between the porin proteins was obtained by doing pairwise comparisons with the SIM sequence analysis tool of Expasy from Swiss-Prot. The comparison matrix used for SIM was BLOSUM62 with the parameters being one alignment computed, a gap open penalty of zero and a gap extension penalty of zero. As shown in Table 1.1, the greatest sequence similarity exists between OmpF and PhoE porins having 53.4% similarity

Table 1.1. Pairwise comparisons of the sequence similarity between the OmpF, PhoE, *N. crassa* and *S. cerevisiae* porins. Sequence comparisons were made using BLOSUM62 with a gap open penalty of zero and a gap extension penalty of zero.

Comparison	Sequence Similarity
OmpF and PhoE	53.4%
<i>N. crassa</i> porin and <i>S. cerevisiae</i> porin	36.2%
OmpF and <i>N. crassa</i> porin	27.0%
OmpF and <i>S. cerevisiae</i>	24.9%
<i>N. crassa</i> porin and PhoE	25.9%
<i>S. cerevisiae</i> and PhoE	24.8%

and the lowest sequence similarity was found between *S. cerevisiae* porin and PhoE porin at 24.8%. The other sequence similarity comparisons between bacterial porins and mitochondrial porins also yielded similar results. The sequence similarity between *N. crassa* porin and *S. cerevisiae* porin was 36.2% which is only 11% higher than the sequence similarity between the different types of porins, but *N. crassa* porin and *S. cerevisiae* porin are both 283 amino acids long indicating an important size conservation for mitochondrial porins.

1.5.2. Structural properties of OmpF porin

Unlike mitochondrial porin, the three dimensional structure of OmpF porin has been solved to 2.4 Å by using single isomorphous replacement (SIR) (Cowan *et al.*, 1992). Crystals were soaked in 2mM platinum-ethylenediamine-dichloride for eight days and phases were calculated using the programs REFINER and Phase. Solvent flattening was then used to improve the 3.0 Å SIR phases to 2.4 Å (Cowan *et al.*, 1992).

The porin channel is formed by a 16-stranded antiparallel β -barrel such that the strands have a tilt angle between 35° and 50° relative to the barrel axis (Fig. 1.4). A pseudo-cyclic structure is formed because of a salt bridge linkage between the amino and carboxy termini in the first and 16th β -strands (Cowan *et al.*, 1992). The end of the barrel that faces the periplasmic space is referred to as the smooth end because of the β -hairpin turns located there while the other end, which faces the cell surface, is referred to as the rough end because of the long irregular loops located in that region. The pore is off center with an angle of 16° relative to the barrel axis while the loops, which are tightly packed, face toward the barrel axis. Loop L3 is a long loop which constricts pore size half way up

Fig. 1.4. The three dimensional structure of the *E. coli* OmpF porin (Cowan *et al.*, 1992).

Image generated using Rasmol.



the barrel and contains 1.5 turns of α -helical structure that fold into the barrel, which results in a gap between strands $\beta 4$ and $\beta 7$.

The formation of the trimeric OmpF porin is favored by hydrophobic interactions where there is an orthogonal stack of β -sheets at the subunit interface due to the twist of the β -strands. Loop L2 is also involved in numerous hydrophilic interactions that hold the trimer together. Loop L2 fits in between L2' and L4' (' denotes location of neighboring subunit of trimer) of the adjacent monomer filling the void left by L3'. Site-directed mutagenesis studies have shown that residue E71 on loop L2 is very important in trimer stability (Phale *et al.*, 1998). The trimer also has tight packing of hydrophobic residues along its symmetry axis not allowing any space for water along the subunit interfaces, instead water is located near the external surface exposed parts of porin. The salt bridge connection between the amino and carboxy termini is hidden from the lipid phase of the membrane by being located at the interface between two monomers. It appears that both the carboxy terminal residue and β -strand 16 are important to the trimer as deletions of these regions disrupts the trimer (Cowan *et al.*, 1992). For each isolated monomer, 35% of the monomer surface is involved in either hydrophobic or hydrophilic subunit interactions allowing porin to be very stable in organic solvents and high concentrations of chaotropic agents (Cowan *et al.*, 1992).

The outer surface of porin features a pronounced segregation of hydrophilicity. The OmpF trimer is surrounded by a hydrophobic band of width 25 Å (Cowan *et al.*, 1992). The outer surface's hydrophilic areas are quite distinct in size. The residues in the β -hairpin that turn at the smooth end of the barrel are mostly negatively charged and interact

with lipid head groups. In contrast, the charge distribution of the residues in the rough end of the barrel is not as uniform, and the area is hydrophilic and larger in size (Cowan *et al.*, 1992). There is a cluster of carboxyl groups at the rough end which might interact with the lipopolysaccharide (LPS) through interactions with divalent cations. The β -barrel has a closed topology to ensure that all of the main chain polar groups are involved in hydrogen bonding between strands and not accessible to the core of the lipid bilayer. Within the OmpF trimer, a hydrophobic core as thick as 15 Å around the axis of symmetry also contributes to the stability of OmpF. The internal loop organization also contributes to porin stability (Cowan *et al.*, 1992).

The transmembrane channel is an aqueous pore whose lining is analogous to the external surface of water-soluble proteins. The shell of the pore is made up by the 16-stranded β -barrel. The pore entrance is narrow due to the rough end of the barrel's long loops. Loop L3 is responsible for compressing the pore to an elliptical cross-section with dimensions 11x7 Å (Cowan *et al.*, 1992). This compression takes place half way up the barrel. Deleting residues 109-114 from loop L3, which are involved in interactions in the constriction zone, resulted in a larger cross-section at the constriction zone but did not effect the overall structure of the β -barrel (Lou *et al.*, 1996). However, the deletion mutant did display a 30% reduction in channel conductance and an altered ion-selectivity (Saint *et al.*, 1996). Beyond the constriction zone, the pore's diameter increases to 15x22 Å indicating that the pore must be in an open state within the crystals (Cowan *et al.*, 1992).

Many of the structural models for mitochondrial porin are based on the structural

properties of OmpF porin discovered from its three-dimensional structure. Without the three dimensional structure of mitochondrial porin, no detailed comparisons could be made between the two structures.

1.5.3. Functional comparisons

There are some differences and similarities in the biological functions of OmpF porin and mitochondrial porin and the manner in which these porins function. OmpF porin forms a water-filled pore, in the outer membrane of *E. coli*, which allows the uninhibited diffusion of small hydrophilic nutrients and waste products similar to mitochondrial porin. One difference between the two porins is that OmpF porin only allows the passage of molecules less than 600 Da across the outer membrane (Forst *et al.*, 1995) while mitochondrial porin allows the passage of molecules up to 4 kDa in the open state (Troll *et al.*, 1992). OmpF porin has no binding sites for specific substrates but seems to be weakly cationic selective (Cowan *et al.*, 1992), in contrast to mitochondrial porin in its open state but similar to it in its closed state. The electrostatic fields at the entrance of the pore for OmpF are responsible for OmpF being cation selective (Jap and Walian, 1996). It can be assumed that the anion-selectivity of mitochondrial porin is also determined, at least in part, by the residues at the entrance of the pore.

The manner in which OmpF porin and mitochondrial porin function is also somewhat different. Both porins are considered to be a nonspecific passive channel because they do not require energy in the form of ATP hydrolysis. However, OmpF allows the diffusion of a wide range of positively or negatively charged solutes (Jap and Walian, 1996), while mitochondrial porin in its open state is slightly selective to negatively charged

solutes and in the closed state is slightly selective to positively charged solutes. The OmpF porin is functional as a trimer unlike mitochondrial porin which likely functions as a monomer.

Since the OmpF porin structure has been solved, detailed studies of how transport occurs through the channel have been possible. The organization of the water molecules within the pore also plays a critical role in the transport of solutes for OmpF porin (Jap and Walian, 1996). In considering the role of water, the model put forward states that if the water molecules of the solute hydration shell matches the water network in the pore, it would minimize the difference in conformational energy between the waters (Jap and Walian, 1996). This means that a solute would either be accepted into the channel or rejected away from it based on the solute's ability to match the water network in the pore. Simulations of transport using Brownian dynamics have shown that the electrostatic potential at the positively charged constriction zone of OmpF porin enhances the permeability of cations, while the transport of anions is not retarded (Schirmer and Phale, 1999). At the constriction zone, the cations follow a distinct path that is determined by the segregation of basic amino acid residues (Schirmer and Phale, 1999).

Voltage-gating of bacterial porin channels, similar to that of mitochondrial porin, has been investigated under *in vitro* conditions (Jap and Walian, 1996). Studies that have involved simulations of molecular dynamics have shown that the constriction loop (loop L3) is vulnerable to changes in the electric field and that the changes can induce conformational changes which might explain how the open and closed states of the pore are generated (Jap and Walian, 1996). However, mutagenesis studies on the constriction

loop have shown that constriction loop displacement is not involved in the voltage-gating of OmpF porin (Bainbridge *et al.*, 1998a; Bainbridge *et al.*, 1998b).

OmpF porin channels studied in patch-clamp experiments have been found to partially close at applied potentials of 60 mV with significant pore closure at 100 mV but there was no pore closure at applied negative potentials (Samartzidou and Delcour, 1998). This behavior is not characteristic of all bacterial porins; for example, PhoE porin, which has a high structural homology to OmpF porin (53%), was found to have a directly opposite voltage-dependence such that pore closed at -100 mV but not at positive potentials (Berrier *et al.*, 1997). The voltage-dependence of these porins is quite different from mitochondrial porin which demonstrates a gating response to both positive and negative potentials (see section 1.2.2.). Polyamines have been found to alter the kinetics of pore closure of OmpF porin and to block ion flow by binding inside the pore (Samartzidou and Delcour, 1999).

1.6. Objectives

The first objective of this thesis will be to study the highly conserved GLK motif in both bacterial and mitochondrial porins which is hypothesized to be involved in ATP binding. To examine this hypothesis, a GLE version of the motif will be generated in *N. crassa* mitochondrial porin. The second objective of this thesis will be to study the structure-function relationships of porin due to the absence of a three-dimensional structure. These relationships will be examined through the use of specific deletion versions of the protein. Based on the electrophysiological properties of these mutants, it is hoped that a more concise structural model of mitochondrial porin will be generated.

CHAPTER 2

Materials and Methods

2.1. Bacterial strains and plasmids

All of the bacterial strains, plasmid constructs and bacteriophage used in this study are listed in Tables 2.1 and 2.2. *E. coli* strains CJ236 (Kunkel *et al.*, 1987) and DH5 α (Hanahan, 1983) were utilized in gene construction while strains XL1-Blue (Bullock *et al.*, 1987) or M15 (Villarejo and Zabin, 1974) were utilized for the purification of recombinant porin proteins. The transformed *E. coli* strains were grown on Luria-Bertani (LB) medium and maintained in the presence of the appropriate antibiotics. Ampicillin (100 μ g/ml), chloramphenicol (20 μ g/ml), kanamycin (25 μ g/ml) and tetracycline (10 μ g/ml) were added to cultures of *E. coli* strains expressing *amp^r*, *cam^r*, *kan^r* and *tet^r* respectively.

2.2. Plasmid DNA isolation

Plasmid DNA was isolated by the alkaline lysis method (Sambrook *et al.*, 1989). High quality sequencing-grade DNA was prepared using the Quantum Prep Plasmid Miniprep Kit (BioRad, Mississauga, ON, Canada) or the Qiagen Plasmid Midi Kit (Qiagen Inc., Mississauga, ON, Canada) according to the manufacturer's procedures.

2.3. DNA manipulation

2.3.1. Site-directed mutagenesis

The porin constructs used in this study were derived from the cDNA clone obtained from Kleene *et al.* (Kleene *et al.*, 1987). The cDNA was recloned into a pBluescript SK⁻ vector (Stratagene, La Jolla, CA) and the resulting construct was used for

Table 2.1 *E. coli* strains used in this study

Strain	Characteristics	Reference
CJ236	<i>dut1 ung1 thi-1 relA1</i> pCJ105(<i>cam^r</i> F')	(Kunkel <i>et al.</i> , 1987)
DH5 α	<i>supE44 ΔlacU169 (ϕ80 <i>lacZ</i>ΔM15) <i>hsdR17</i> <i>recA1 endA1 gyrA96 thi-1 relA1</i></i>	(Hanahan, 1983)
M15	<i>na^r str^r rif^r lac⁻ ara⁻ gal⁻ mtl⁻ F⁻ recA⁻ uvr⁻</i> pREP4(<i>lacI kan^r</i>)	(Villarejo and Zabin, 1974)
XL1- Blue	<i>supE44 <i>hsdR17</i> <i>recA1</i> <i>endA1</i> <i>gyrA46</i> <i>thi</i> <i>relA1 lac⁻</i> F' [<i>proAB⁻ lacI^h lacZ</i>ΔM15 Tn10(<i>tef</i>)]</i>	(Bullock <i>et al.</i> , 1987)

Table 2.2 Plasmids and bacteriophage used in this study

Plasmid or Phage	Characteristics	Source
pBluescript SK ⁺	<i>amp^r</i> , Blue/white color screening, Bacteriophage T3 and T7 promoters, ssDNA fl (-) origin of replication	Stratagene
pQE-9	<i>amp^r</i> , <i>E. coli</i> <i>lacP</i> , ribosome binding site, N-terminal His ₆ -tag	Qiagen
R408	Helper phage	Promega

the generation of single-stranded DNA to be used for site-directed mutagenesis (Kunkel *et al.*, 1987). The construct was transformed into *E. coli* CJ236. The transformed cells were subsequently superinfected with helper phage R408 for 6 hours at which time infected cells were removed by centrifugation and the phage were precipitated with a 20% PEG/2.5 M NaCl solution. The T7 mutagenesis kit (BioRad) and mutagenic oligonucleotides (Table 2.3) obtained from Life Technologies (Burlington, ON, Canada) were used to create different porin mutants. Mutagenesis was carried out according to the manufacturer's instructions. In the case of mutagenic oligonucleotide dc22, a new *Xho*I restriction site (CTCGAG) was introduced at the base substitution site (underlined). The sequences of the mutated regions and flanking DNA to be used in further constructions were confirmed by DNA sequencing at the DNA sequencing facility in the Institute of Cell Biology, University of Manitoba.

2.3.2 General cloning methods

To clone the K95E mutant (GLEporin) coding sequence into the expression vector pQE-9 (Qiagen, Hilden, Germany), PCR was first used to amplify a 320-bp fragment encompassing the K95E mutation from pBluescript-GLEporin utilizing a MJ Research MiniCycler (MJ Research Inc., Watertown, MA, USA). The upstream primer (5'AAAGGATCCATGGCTGTTCC-CGCTTTC) incorporates a *Bam*HI site (underlined) at the 5'-end of the PCR product and the second primer (5'CTTGAAGTGGAGGTTGAACTTGGC) hybridizes to a sequence downstream of the endogenous *Nar*I site. The PCR product and the pQE-9-derived plasmid that encodes the wild-type porin, His₆porin (Popp *et al.*, 1996) were then digested with *Bam*HI and *Nar*I

Table 2.3 The mutagenic oligonucleotides used in this study. The underlined sequence indicates where base substitution took place and • where deletions are located.

Primer	Sequence (5'-3')	Mutation
dc22	CAAGGGTCTC <u>G</u> AGGCTGAGGGTATC	K95E
GR3	TCCAGAAGGCTGCCA*GCGCCGCTGTCG	Δ163-166
GR4	CCATCACTGGTTACA*ACCACGCCCTAC	Δ167-171
GR6	CCGCTTCTTACTACC*AGGTTGAGGCCG	Δ196-200
GR9	CCAAGTACCGCATTG*TCAAGGGCAAAGATC	Δ229-233
GR10	TCGTCAAGGGCAAGA*TCGCTGCCATTGCCTAC	Δ238-242
GR11	TCAACGACCGTGGTG*ATGTTCTCCTCCGTG	Δ243-248
GR12	CGGCCACGAGGGTT*CCGCTGGCTACGATG	Δ148-152
GR13	GCCCCTACCTACA*CTACTGACAACCTGAGC	Δ178-182
GR14	CCGCTACTGACAACC*CTTCTTACTACCACAAGG	Δ187-191

according to the manufacturer's instructions and the resulting 293-bp digested PCR fragment and the 4.7 kb digested plasmid fragment were purified by the DEAE cellulose method (Sambrook *et al.*, 1989). Each fragment was purified on a 1% agarose gel, electrophoresed onto a DEAE cellulose membrane (Schleicher and Schuell, Keene, NH, USA) and purified according to the manufacturer's instructions. The purified fragments were then ligated together with T4 DNA Ligase (Life Technologies, Burlington, ON). The resulting plasmid encodes GLEporin, which includes an N-terminal hexahistidiny (His₆) tag. The sequence of the *BamHI-NarI* fragment was confirmed by DNA sequencing.

The porin deletion mutants were cloned into the expression vector pQE-9 by digesting each of the mutant genes in pBluescript and His₆porin with *NarI* and *PstI*. The resulting C-terminal 650-bp fragments and the 4.35 kb pQE-9 plasmid fragment were purified using the DEAE cellulose method and the purified 650 bp fragments were ligated to the plasmid fragments with T4 DNA Ligase (described above). The resulting plasmids encode each of the deletion mutants fused with an N-terminal His₆ tag. The sequences of the mutant fragments were confirmed by DNA sequencing.

2.4. Protein expression and purification

Overnight cultures grown in LB (Sambrook *et al.*, 1989) or DYT (Popp *et al.*, 1996) medium of *E. coli* M15 or XL1-Blue containing the pQE-9 plasmids encoding His₆porin or mutant porins were diluted and grown to an A₆₀₀ of 0.7-0.9. Protein expression and purification by affinity chromatography on Ni-NTA agarose (Qiagen Inc.) were carried out as described by the manufacturer's instructions. Briefly, porin expression was induced by the addition of IPTG (2 mM final concentration) and cells were grown for

4 hours. Cells were then harvested by centrifugation at 4000xg, lysed in Buffer B (8 M urea, 0.1 M NaH₂PO₄, 0.01 M Tris, pH 8.0) and the lysate was incubated with the Ni-NTA agarose resin which binds the His₆ tagged porins. Contaminating proteins were then washed off the resin with Buffer C (8M urea, 0.1 M NaH₂PO₄, 0.01 M Tris-HCl, pH 6.3) and the His₆ tagged porins were eluted by addition of Buffer C/100 mM EDTA. Protein purity was monitored by sodium dodecylsulfate-polyacrylamide gel electrophoresis (SDS-PAGE).

2.5. Sodium dodecylsulfate-polyacrylamide gel electrophoresis

SDS-PAGE was performed using a 14% separating gel underlying a 5% stacking gel (Sambrook *et al.*, 1989). Protein samples were loaded with sample buffer containing 50 mM Tris-HCl, pH 6.8, 7% (v/v) glycerol, 1.3% (w/v) SDS, 0.01% (w/v) bromophenol blue and 0.5% (v/v) β-mercaptoethanol. Samples were heated at 100°C for 7 min prior to loading. Protein samples were electrophoresed alongside a low molecular weight range SDS-Page standard (Sigma, Oakville, ON, Canada) at 100-200 V. Gels were stained for 30 minutes in Coomassie Blue solution (0.1% (w/v) Coomassie Brilliant Blue G-250, 40% (v/v) methanol and 10% (v/v) acetic acid) and subsequently destained overnight with 40% methanol/10% acetic acid.

2.6. Western immunoblotting of Δ163-166 porin

Following SDS-PAGE, a Mini Trans-Blot Transfer Cell (BioRad) was used to transfer Δ163-166 porin onto a Trans-Blot nitrocellulose transfer membrane (BioRad) according to the manufacturer's instruction manual. Protein was transferred at constant current of 250 mA for 1 hour in transfer buffer containing 25 mM Tris-HCl, pH 8.3, 192

mM glycine and 20% (v/v) methanol. Immunodetection of Δ 163-166 porin was carried out by using a general immunoblotting procedure (Bollag and Edelstein, 1991). The blotted membrane was first incubated at room temperature in TBS buffer (10 mM Tris-HCl, pH 7.5, 150 mM NaCl) containing 5% (w/v) skim milk for 30 minutes at which time a 1:1000 dilution of anti-porin antiserum (generously provided by Dr. R. Lill, Universitaet Muenchen) was added for 1 hour. Subsequently, goat-anti-rabbit IgG conjugated to horseradish peroxidase (Sigma, Oakville, ON, Canada) was added to the membrane at a dilution of 1:5000 for an additional 1 hour. The blot was then treated with Luminol reagents 1 and 2 (Amersham Life Science Inc., Oakville, ON, Canada) and exposed to Kodak (X-OMAT) film for 45 seconds for detecting protein bands.

2.7. Preparation of porin proteins for biochemical and biophysical analysis

The purified proteins used for biophysical analysis were diluted 1:10 in 1% Genapol X-80 (Fluka, Buchs, Switzerland), 1 mM EDTA, 10 mM potassium phosphate, pH 7 and dialyzed against the same buffer. The purified protein used for cross-linking studies was diluted 1:2 in 1% Genapol X-80, 10 mM potassium phosphate, pH 7 and dialyzed against the same buffer. Protein used for circular dichroism (CD) measurements was diluted 1:2 into 1% Genapol X-80, 10 mM potassium phosphate, pH 7 and concentrated in a Centricon 10 column (Amicon, Inc., Beverly, MA) before extensive dialysis against the same buffer.

2.8. Concentrating of protein on Centricon columns

Protein was concentrated in Centricon 10 columns according to the manufacturer's instructions. Centricon 10 columns contain a membrane with an exclusion limit of 10 kDa.

Protein was diluted 1:2 in dialysis buffer (described above) and loaded into Centicon 10 columns. Samples were centrifuged at 2500xg in a Sorvall SS34 rotor for 75 minutes at room temperature at which time the sample in the filtrate vial was discarded and the retentate containing porin protein was collected.

2.9. Cross-linking of purified His₆porin and GLEporin to [³²P]-ATP through periodate oxidation

Approximately one hundred nanograms of purified His₆porin and GLEporin were diluted in PBS (137 mM NaCl, 1.5 mM KH₂PO₄, 16.6 mM K₂HPO₄, 5.4 mM KCl, pH 7.4) containing 10 mM MgCl₂ to a volume of 100 µl, and incubated with 10 µCi of [α -³²P]ATP (3000 Ci/mmol; New England Nuclear, Boston MA USA) for 10 minutes at room temperature. Samples were then incubated in the presence or absence of cross-linking reagents as described by (Rudel *et al.*, 1996). Briefly, the [α -³²P]ATP was oxidized by addition of 1 mM NaIO₄, reduced with NaCNBH₃ and the reaction was stopped with NaBH₄ (Peter *et al.*, 1992). Subsequently, proteins were precipitated with nine volumes of ice-cold acetone, washed twice with 70% acetone, resuspended in loading buffer and separated by SDS-PAGE. Gels were stained with Coomassie Brilliant Blue and then dried. The dried gels were exposed to Kodak (X-OMAT) film for 10 days.

2.10. Lipid bilayer experiments

The lipid bilayer experiments were performed by Elke Maier from the Roland Benz lab (Universitaet Wuerzburg). The methods used for the “black” lipid bilayer experiments have been previously described (Benz *et al.*, 1978). In short, membranes were made by application of a 1% (w/v) solution of diphytanoyl phosphatidylcholine (DiphPC, Avanti

Polar Lipids, Alabaster, AL) in *n*-decane across circular holes with a surface area about 0.1 mm² in the thin wall of a Teflon cell which separates two 5-ml aqueous compartments. The aqueous solutions were either buffered with 10 mM N-[2-hydroxyethyl] piperazine N'-[2-ethane-sulfonic acid (HEPES) to pH 7 or unbuffered at pH 6. Dialyzed protein solution, containing 0.5% (w/v) ergosterol, was added to the aqueous phase in the *cis*-compartment where the voltage was applied after the membranes had turned optically black in reflected light.

2.11. Circular dichroism

CD spectra were obtained using a JASCO J-500A spectropolarimeter calibrated with (+)-10-camphorsulfonic acid. The instrument was purged with N₂ at 5 l/min above 210 nm and at 25 l/min below 210 nm. Spectra were measured, in a quartz cell with a 0.5-mm path length, at a scan rate of 2 nm/min with a time constant of 8 s above 210 nm and at 0.5 nm/min with a time constant of 32 s for spectra below 210 nm. The concentrations of His₆porin and GLEporin samples were determined from their molar extinction coefficients and absorbance at 280 nm.

The secondary structures of His₆porin and mutant porins were determined using the convex constraint algorithm (CCA) of Perczel *et al.* (1992). The CD spectra of His₆porin and GLEporin were individually appended to the membrane-protein reference data set of Park *et al.* (1992) for deconvolution by CCA.

CHAPTER 3

GLEporin Mutant Results and Discussion

Mitochondrial porin facilitates the diffusion of small hydrophilic molecules across the mitochondrial outer membrane. Despite low sequence similarity among porins from different species, channel properties such as voltage dependence, ion selectivity and single channel conductance are highly conserved. In addition, the proteins are predicted to possess similar secondary structures, containing stretches of alternating hydrophobic and hydrophilic amino acids that suggest the formation of amphipathic β -strands (Benz, 1994; Blachly-Dyson *et al.*, 1990; De Pinto *et al.*, 1991). A glycine-leucine-lysine (GLK) motif is highly conserved among mitochondrial porins from different species and in *Neisserial* porins (Troll *et al.*, 1992; Fig. 3.1). It has been proposed that these residues are involved in the binding of the purine nucleotides ATP and GTP because the motif resembles the GTP binding site in the T cell receptor ζ chain (Rudel *et al.*, 1996). In the latter protein, the lysine residue in a glycine-methionine-lysine (GMK) motif was found to be the site to which GTP could be chemically cross-linked (Peter *et al.*, 1992). To investigate the possible role of these conserved residues in ATP binding by the protein, the lysine residue of the GLK motif of *Neurospora crassa* porin was replaced with glutamic acid through site-directed mutagenesis to create a glycine-leucine-glutamate (GLE) sequence. The electrophysiological and structural properties of the mutant GLEporin are also studied and compared to that of the wild type.

3.1. Site-directed mutagenesis

To study the possible function of the GLK motif, including its possible role in ATP

Fig. 3.1. The conserved GLK motif. The amino-acid sequences of the indicated porins were aligned using the Clustal 1.7 software (Thompson *et al.*, 1994); a short sequence including the conserved GLK (bold text) is presented here. The number to the left of the sequence alignment indicates the position of the adjacent residue in the corresponding protein sequence.

Organism/Porin Swiss-Prot	Sequence
<i>Neurospora crassa</i> Porin1 P07144	83 KVEMADNLA KGLK AEGIFSFLPA
<i>Saccharomyces cerevisiae</i> Porin1 P04840	83 KLEFAN-LTP GLK NELITSLTPG
<i>Saccharomyces cerevisiae</i> Porin2 P40478	82 RIEFSK-IAP GWK GDVNAFLTPQ
<i>Solanum tuberosum</i> (Potato) POM34 P42055	82 TITVDE-AAP GLK TILS-FRVPD
<i>Solanum tuberosum</i> (Potato) POM36 P42056	95 TITVDE-PAP GLK TIFS-FVVPD
<i>Triticum aestivum</i> (Wheat) Porin1 P46274	95 TITADDLAAP GLK TILS-FAVPD
<i>Dictyostelium discoideum</i> Porin1 Q01501	109 EFTIEN-IIP GLK AVAN----GD
<i>Xenopus laevis</i> Porin2 P81004	82 EIAIEDQIA KGLK LTFDITTFSPN
<i>Mus musculus</i> (Mouse) Porin1 Q60932	83 EITVEDQLAR GLK LTFDSSSFSPN
<i>Mus musculus</i> (Mouse) Porin2 Q60930	78 EIAIEDQICQ GLK LTFDITTFSPN
<i>Mus musculus</i> (Mouse) Porin3 Q60931	78 EISWENKLA EGLK LTLDTIFVPN
<i>Rattus norvegicus</i> (Rat) Porin2 P81155	78 EIAIEDQICQ GLK LTFDITTFSPN
<i>Homo sapiens</i> Porin1 P21796	82 EITVEDQLAR GLK LTFDSSSFSPN
<i>Homo sapiens</i> Porin2 P45880	81 EIAIEDQICQ GLK LTFDITTFSPN
<i>Neisseria gonorrhoeae</i> PorB P18195	99 TGWGNKQSFV GLK GGFGTIRAGS
<i>Neisseria meningitidis</i> PorB P30687	99 SGWGNRQSF I GLK GGFGKLRVGR

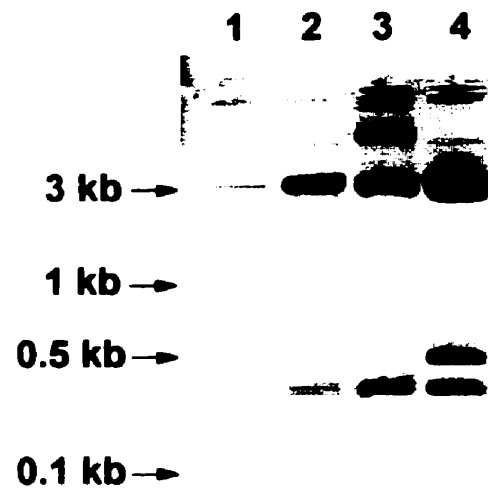
binding, site-directed mutagenesis was performed to change the lysine residue of the motif into a glutamic acid to create a mutant with the altered motif of glycine-leucine-glutamate (GLEporin). Mutagenesis of the corresponding codon was achieved by making use of the phagemid system (Kunkel *et al.*, 1987). A cDNA clone of the porin gene in pBluescript SK⁻ was used to generate single-stranded DNA (ssDNA) after co-infection with the helper phage R408. The ssDNA of the cDNA clone was annealed by the mutagenic primer dc22 (Table 2.3) which creates a new *Xho*I restriction site at the base substitution site (see materials and methods) and second strand synthesis was carried out by T7 DNA polymerase. The double-stranded hybrid was then transformed into *E. coli* DH5 α and plasmid DNA from potential mutant colonies was screened by *Xho*I digestion for the mutation (Fig 3.2). DNA containing the new *Xho*I site was sequenced to confirm the mutation and ensure that further mutations were not introduced into the gene.

3.2. Cloning of the GLEporin mutant into pQE-9

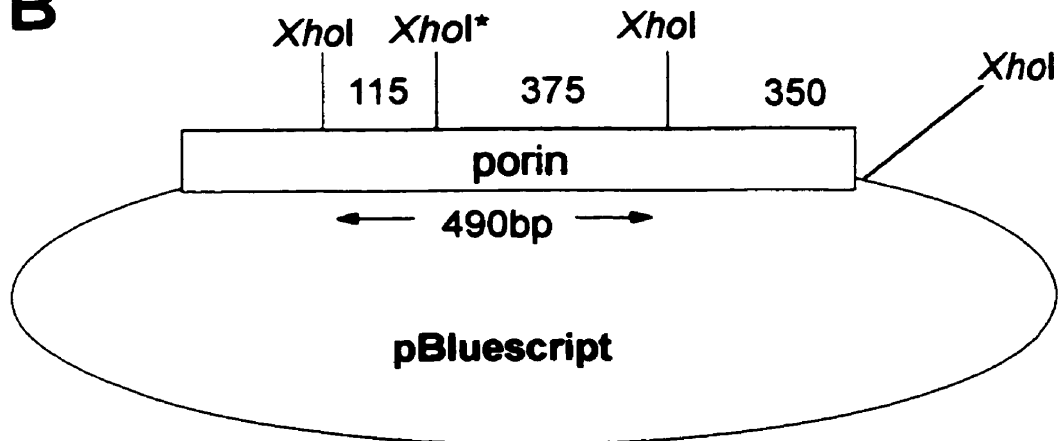
In order to be able to express and purify the GLEporin mutant, a portion of the mutant gene from pBluescript SK⁻ was used to replace the corresponding DNA in His₆porin from the plasmid pQE-9 (Qiagen). Since pQE-9 contains an inducible *E. coli* *lacP* (Table 2.2) which we desire to retain, PCR was performed to amplify the N-terminal part of the mutant gene to produce a 320-bp fragment with a 5' *Bam*HI site introduced with the primer. The resulting product was digested with *Bam*HI and *Nar*I to produce a 293-bp fragment containing the mutation. The 293-bp mutant fragment was used to replace the corresponding fragment from His₆porin, which was also digested with *Bam*HI and *Nar*I. The resultant pQE-9 derived plasmid construct encodes GLEporin with an

Fig. 3.2. (A) Ethidium bromide stained 2% agarose gel of the *Xho*I-digested pBluescript SK⁻ plasmids containing the coding sequences for the GLEporin mutant (lanes 2 and 3) and wild-type porin (lane 4). Lane 1 was loaded with the 100-bp DNA ladder (BioRad). The 485-bp product from the wild-type (lane 4) is digested into a 370-bp fragment that co-migrates with the 350-bp fragment and a 115-bp fragment (lanes 2 and 3) due to the new *Xho*I site in the mutant. Note the absence of the 115-bp band in lane 4. Digestion products over 3 kb represent partial digestion. **(B)** Restriction map of pBluescript SK⁻ containing cDNA for the GLEporin mutant. The *Xho*I restriction sites along with the expected band sizes are shown. *Xho*I^{*} indicates the new *Xho*I site created in the GLEporin mutant. Fragment sizes are given in bp.

A



B



N-terminal His₆ tag whose expression is under the control of the inducible *lacP*. Clones were screened by *Xho*I digestion and positive clones were sequenced to confirm the inserted 293-bp *Bam*HI/*Nar*I mutant fragment derived from PCR.

3.3. GLEporin expression, purification and dialysis

Porin expression was induced by the addition of IPTG to *E. coli* XLI-Blue cells that had been transformed with the pQE-9 construct containing GLEporin. Cells were then lysed with urea and the His₆ tagged GLEporin was purified on Ni-NTA agarose. The purified GLEporin was eluted from the resin as described in section 2.4 and purity was monitored on SDS-PAGE (Fig 3.3). A small amount of contaminating proteins was detected (Fig. 3.3), however these amounts were too small to affect the analyses of GLEporin. After confirming GLEporin purity, protein was diluted either 1:2 or 1:10 with dialysis buffer (section 2.7.), depending on the method of analysis being performed, and subjected to dialysis (Fig. 3.3). Dialysis into Genapol X-80 is required to allow the porin to be able to fold before doing biophysical and biochemical analysis. In the case of the protein used for CD, it was concentrated on a CentriconTM column before being dialyzed (Fig. 3.3).

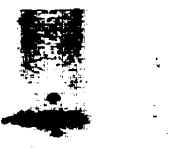
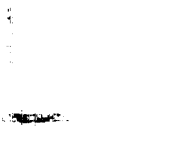
3.4. ATP binding by GLEporin

Chemical cross-linking utilizing purified porin and [α -³²P]-ATP was used to determine if GLEporin, like His₆porin, is capable of binding ATP. As shown in Fig. 3.4, purified His₆porin was covalently labelled by [α -³²P]-ATP in reactions containing cross-linking reagents, indicating that His₆porin is capable of binding ATP and that the N-terminal His₆ tag does not disrupt this binding. GLEporin was also covalently bound to

Fig. 3.3. Coomassie Blue stained SDS-PAGE of GLEporins. Lane 1, Low Molecular Weight Marker (Sigma); lane 2, GLEporin eluted in urea-containing buffer from Ni-NTA resin; lane 3, dialyzed after purification to be used for ATP binding experiments; lane 4, concentrated on Centricon 10TM column after purification, then dialyzed (lane 5) to be used for circular dichroism studies. Each lane was loaded with 10 µl of protein.



Fig. 3.4. Covalent coupling of [α - 32 P]ATP to His₆porin and GLEporin. His₆porin and GLE porin were incubated with [α - 32 P]ATP and chemically cross-linked (+ X-L). As a negative control, His₆porin and GLE porin were incubated with [α - 32 P]ATP in the absence of cross-linker (- X-L). Samples were analyzed by SDS-PAGE; autoradiographs of the dried gels are presented. Numbers to the left of the figure indicate the positions of molecular weight markers run on the same gel.

Porin	His ₆ porin		GLEporin	
X-L	+	-	+	-
45— 36— 29—				

[α - 32 P]-ATP (Fig. 3.4), demonstrating that the conserved GLK motif is not essential for ATP binding by *N. crassa* mitochondrial porin.

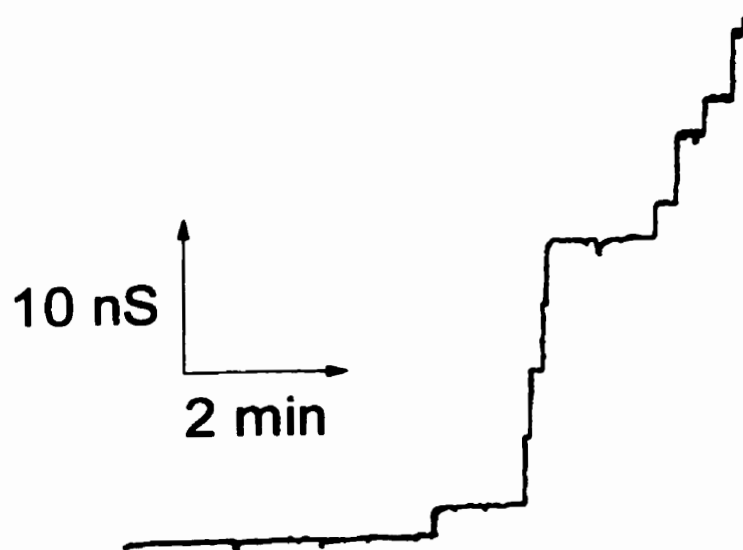
3.5. Single channel properties of GLEporin

The electrophysiological properties of GLEporin were examined and compared to those of wild type porin to determine if the conserved GLK motif was critical for these characteristics. Previous studies have shown that the His₆tag does not change the electrophysiological characteristics of His₆porin compared to the native porin (Koppel *et al.*, 1998; Popp *et al.*, 1996). The single channel readings generated from GLEporin (Fig. 3.5A) are similar to those from His₆porin (Popp *et al.*, 1996). The conductance increase produced by both proteins occurs in distinct steps of similar amplitudes. The majority of the conductance steps are at 1 nS and between 4 and 5 nS for GLEporin (Fig. 3.5B) similar to those of His₆porin (Popp *et al.*, 1996). The voltage-dependent gating of the channels formed by the GLEporin mutant was also examined (Fig. 3.6). G_U/G_O is the ratio of the conductance, G_U , at a given voltage, U , divided by G_O at 10 mV is shown as a function of voltage. GLEporin was found to be similar to that of His₆porin at applied voltages of greater than 30 mV; for example, the G_U/G_O of GLEporin at 50 mV was 0.52 compared to 0.43 for His₆porin (Popp *et al.*, 1996). However, the GLEporin appeared to be slightly less sensitive to gating at very low negative voltages (-20 mV).

If the GLK motif is located within a β -strand, changing a lysine into a glutamate would alter the charge within the pore and could alter the ion selectivity of the pore. The GLEporin channels are cation selective (P_C/P_A of 1.4), in contrast to the anion-selective

Fig. 3.5. (A) Single channel recording of GLEporin inserted into diphytanoyl phosphatidylcholine/*n*-decane membranes. 2.5 ml of GLEporin (2-30 ng/ml with 0.5% ergosterol in 1% Genapol X-80 buffer) were added to the *cis* compartment. Addition of the protein took place before the recording. **(B)** Histogram of the conductance fluctuations of GLEporin inserted into black lipid bilayers. $p(G)$ is the frequency that a given conductance increment G is observed in the single channel experiment. $p(G)$ was calculated by dividing the number of fluctuations with a given conductance increment by the total number of conductance fluctuations. The aqueous phase contained 1 M KCl (pH 6.0). The applied membrane potential was +10 mV; $T = 20^{\circ}\text{C}$. The number of observed conductance increments was 251.

A



B

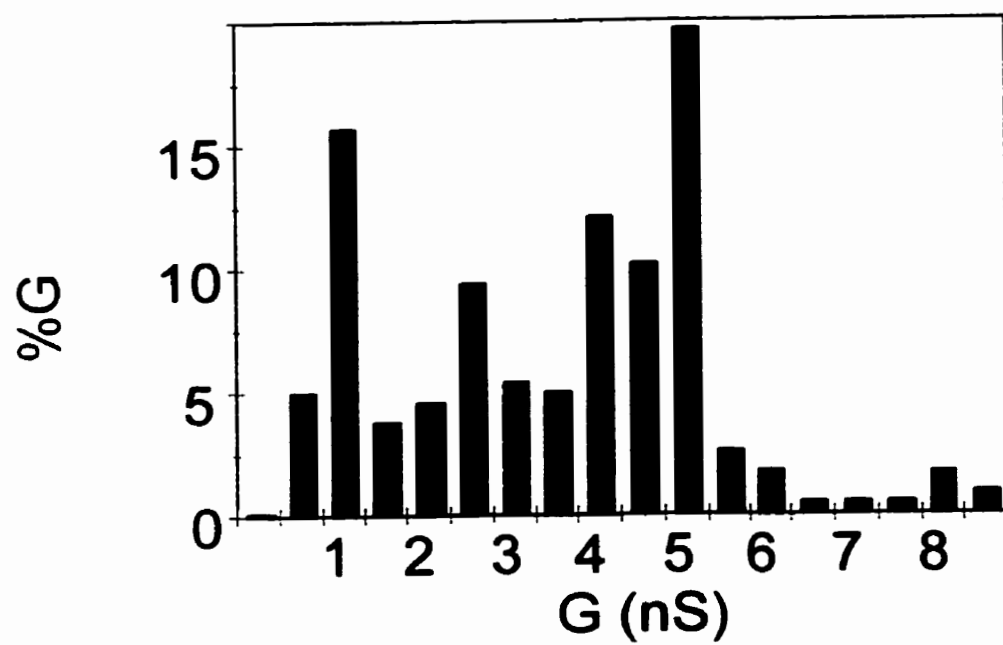
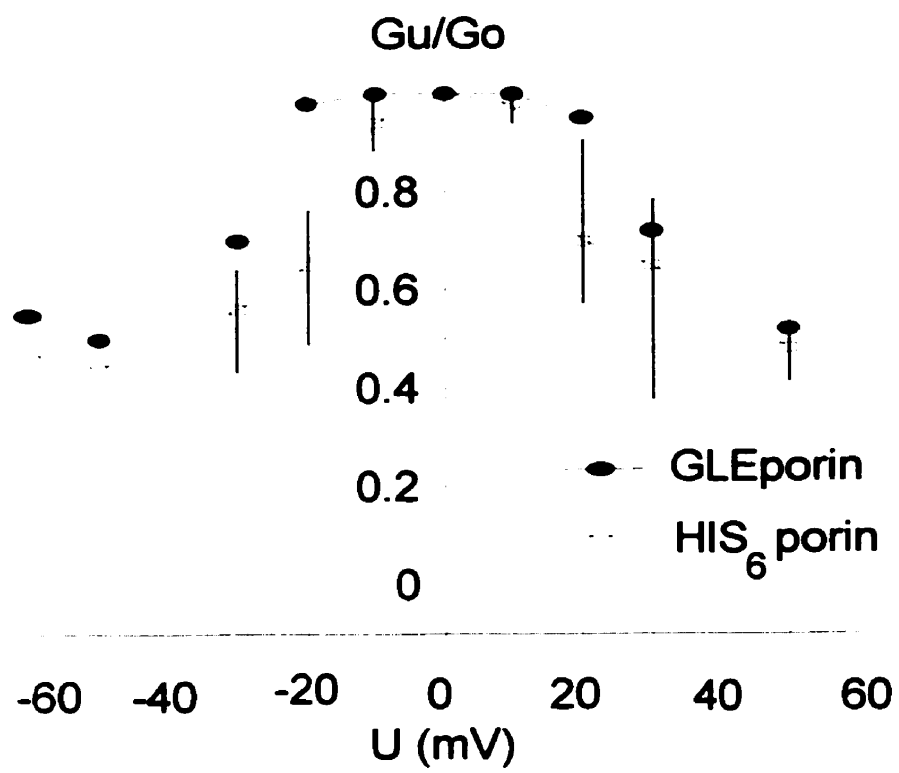


Fig. 3.6. Voltage dependence of His₆porin and GLEporin conductance. Experiments were repeated between two and four times; the average G_v/G_o values are plotted. The data for His₆porin (\square) are replotted from (Popp *et al.*, 1996), vertical lines indicate the standard deviation of the data points. Standard deviations for the GLEporin data (\bullet) were all less than 3% of the plotted data and therefore too small to be indicated on the plot. The membranes were formed of DiphPC/*n*-decane. The aqueous phase contained 1 M KCl (pH 6.0); T = 20°C.



native wild-type porin and His₆porin, for which the P_C/P_A values are 0.77 and 0.67, respectively (Popp *et al.*, 1996). The effect of ATP on ion selectivity was also studied; binding of this negatively-charged molecule to the inside of the pore would likely have an effect on the charge distribution of the lining of the pore, and hence its ion selectivity. A five-fold KCl gradient was established across a porin-containing black lipid membrane, and buffered ATP was added, to a final concentration of 5 mM, to the chamber containing the dilute KCl solution. Zero current membrane potential was measured, and used to determine ion selectivity. In the presence of ATP, P_C/P_A for native and His₆porin was 3.5, compared to 0.6 in the absence of ATP. An increase in cation selectivity was also observed for GLEporin. The presence of ATP increased P_C/P_A from 1.6 to 5. These results suggest that ATP binding has a similar net effect on the ion selectivity of both GLEporin and the wild-type protein.

3.6. Circular dichroism studies

To determine if the conserved GLK motif is critical to porin structure, the circular dichroism spectra of GLEporin and wild type porin were compared. The CD spectra of His₆porin and GLEporin are presented in Figure 3.7A. Spectra of His₆porin and GLEporin show broad minima with negative peaks at 215 nm and 218 nm, respectively (Table 3.1). The wavelengths at which the molar ellipticities are zero ($\lambda_{\text{crossover}}$) are also similar for the two proteins: 207.5 nm for His₆porin and 209.5 nm for GLEporin. The CD spectra of His₆porin and GLEporin further were analyzed to determine the relative contributions of pure structural components to the spectra. The CCA algorithm by Perczel *et al.* (1992) was used, and data for each porin were appended individually to the membrane protein

Fig. 3.7. Circular dichroism analyses of His₆porin and GLEporin. **(A)** The experimentally measured data for His₆porin (0.027mg/ml) and GLEporin (0.066 mg/ml) (□ and O, respectively) and those calculated from the weighted pure component curves (solid and dashed lines, respectively) produced by convex constraint algorithm (CCA) analysis (Perczel *et al.*, 1992) are presented. Pure component curves generated by CCA analysis of His₆porin **(B)** and GLEporin **(C)** are also presented; □, α helix; solid line, α_i helix; O, β sheet; Δ, random coil. Note that the spectrum for wild-type porin does not contain α_i structure and therefore there is not a curve representing this component in **(B)**.

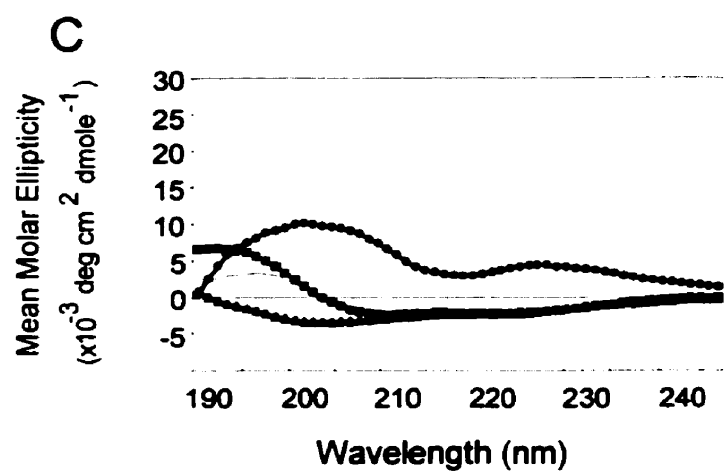
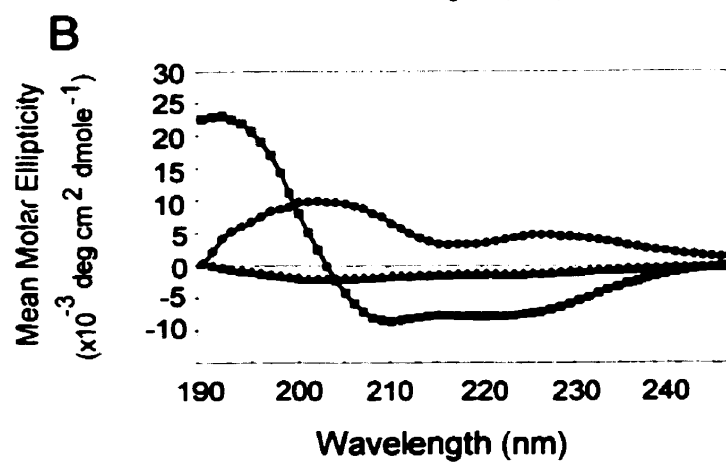
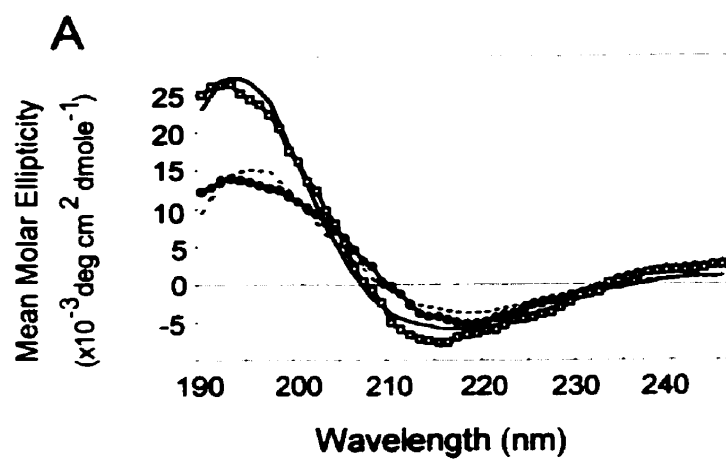


Table 3.1. Compilation of circular dichroism data obtained from *Neurospora* porins.

Porin	Conditions	$\lambda_{\text{crossover}}$ (nm)	λ_{min} (nm)	α - helical content (%)	β -strand content (%)	Other (%)	Reference
His ₆ porin	1% Genapol X-80, pH 7	207.5	215	31 ^a	47	22 ^b	this work
GLEporin	1% Genapol X-80, pH 7	209.5	218	15 ^a	47	38 ^b	this work
His ₆ porin	1% LDAO ^c , pH 8	205	216	12	45	37 ^d	(Koppel <i>et al.</i> , 1998)
Native porin	1% LDAO, pH 8	205	214	12	45	37 ^d	(Koppel <i>et al.</i> , 1998)
Native porin	2% β -OG ^e , pH7	205.5	216	30	62	8 ^d	(Shao <i>et al.</i> , 1996)

^a includes transmembrane helix (α_c)

^b random coil

^c lauryl dimethylamine oxide

^d β -turn plus random coil

^e β -octoylglucoside

data set of Park *et al.* (1992). Initially, the number of pure component curves (P) comprising the data sets were determined *a priori*. We analyzed both sets of data, using 2, 3, 4, or 5 for the value of P. When P = 2, 3 or 5, one or more of the pure component curves was unidentifiable for both proteins. For P = 4, however, all of the pure curves correspond to the spectra arising from pure secondary structures (Perczel *et al.*, 1992). Figures 3.7B and 3.7C show the pure component curves generated for His₆porin and GLEporin for P = 4. In this case the curves correspond to α helix, transmembrane α helix (α_t helix), β sheet and random coil. The estimated amounts of these four structures for His₆porin are 31% α helix, 0% α_t helix, 47% β sheet and 22% random coil (Table 3.1). For GLEporin (Fig. 3.7C and Table 3.1), the estimate of β -sheet content is similar, 47%, and the amount of transmembrane α -helix is also very low (6%). However, the α -helical content in GLEporin is lower (9%) than in His₆porin (31%); this decrease is accompanied by a comparable increase in random coil structure to 38%.

3.7. Discussion

3.7.1. Single channel conductance, voltage gating and ion selectivity of the GLE mutant

The GLEporin forms stable open channels that display normal voltage-dependent gating, but are more cation-selective than the wild-type His₆porin. A similar change in ion selectivity was reported for the equivalent GLEporin of *Saccharomyces* (Blachly-Dyson *et al.*, 1990). The altered ion selectivity suggests that the GLK motif is located within a β -strand that forms the pore lining, where it would contribute to the net charge of the water-exposed surface inside the pore. This location of the GLK motif is in agreement

with the current structural models of *N. crassa* mitochondrial porin (Benz, 1994; De Pinto *et al.*, 1991; Mannella *et al.*, 1992; Popp, 1996; Song and Colombini, 1996) and *Neisseria* PorB (Derrick *et al.*, 1999), which position this motif in the β -barrel of the protein, near the junction of the barrel and a membrane-exposed loop. However, without high resolution structural data, it cannot be ruled out that this motif is located in a cytoplasmically-exposed loop that contributes to ion selectivity through a long-range electrostatic effect.

3.7.2. Interactions of GLEporin with ATP

The experiments presented herein demonstrate that the His₆porin (Fig. 4), like native porin purified from mitochondria (Rudel *et al.*, 1996), binds ATP, which can be subsequently cross-linked to the protein via periodate oxidation. Thus, the hexahistidiny tag, engineered onto the N-terminus of the protein for purification purposes, does not interfere with ATP binding or the subsequent cross-linking reaction. GLEporin was also cross-linked to ATP, indicating that the replacement of the lysine residue by glutamate does not disrupt ATP binding to mitochondrial porin. This conclusion is supported by the observation that GLEporin, like the wild-type molecule, becomes more cation selective in the presence of ATP, as expected if a negatively-charged molecule is bound either within the channel, or in the vicinity of the opening of the pore. Taken together, these results suggest that, although the GLK motif resembles the GMK motif in the T cell receptor ζ chain that is important for GTP binding (Peter *et al.*, 1992), it is not part of the ATP-binding site of mitochondrial porin.

3.7.3. Circular Dichroism

As summarized in Table 3.1, the CD spectrum of wild-type His₆porin in Genapol X-80 is very similar to the spectra observed by Shao *et al.* (1996) for native *Neurospora* porin in 2% β -octoylglucoside (β -OG) pH 7, and in lauryl dimethylamine oxide (LDAO) pH 8 (Koppel *et al.*, 1998), and for recombinant pea root plastid porin in Genapol X-80 (Popp *et al.*, 1997). The CD results are also similar to those of His₆porin created by Koppel *et al.* (1998) and examined at pH 8 in LDAO (Table 3.1). Thus, mitochondrial porin maintains high β -content in a variety of detergents between pH 7 and pH 8. Furthermore, the addition of 12 (this work) or 20 (Koppel *et al.*, 1998) amino-acid residues, including the hexahistidiny tag, does not alter this characteristic. Although these results support models for mitochondrial porin based on a β -barrel structure, the lack of information concerning the length of each β -strand does not allow the calculated β -sheet content to be used as a criterion for excluding or supporting the models for porin currently presented in the literature (see Introduction).

Deconvolution of the CD spectrum of the mutant GLEporin also indicates that the β -strand content of this protein, in detergent, is identical to that of the native porin (47%; Table 3.1). Thus, the detergent appears to promote the folding of similar β -strand structures in the wild-type and mutant proteins, an observation in agreement with the similar electrophysiological properties of the two proteins. However, there are small differences in the amounts of total α -helix and random coil structure between His₆porin (31% and 22%, respectively) and GLEporin (15% and 38%), which are not reflected in the behaviour of GLEporin in black lipid bilayers. Presumably, these structural differences

affect the exposed loops of the protein, and if so, these results may indicate that detergent and lipid membranes promote slightly different folding of these parts of the molecule in the GLEporin.

In summary, the GLK motif is not essential for pore-formation or ATP-binding by mitochondrial porins. The lysine residue does contribute to the anion-selective nature of the pore, suggesting a possible reason for conservation of the motif in many mitochondrial porins.

CHAPTER 4

Functional Characterization of Porin Mutants

Mitochondrial porin, which facilitates the diffusion of small hydrophilic molecules across the mitochondrial outer membrane, has a low sequence similarity between different species. Despite this low sequence similarity, channel properties such as voltage dependent gating, ion selectivity and single-channel conductance are highly conserved. In addition, the proteins are predicted to possess similar secondary structures, containing stretches of alternating hydrophobic and hydrophilic amino acids that suggest the formation of amphipathic β -strands (Benz, 1994; Blachly-Dyson *et al.*, 1990; De Pinto *et al.*, 1991). To test the current structural models of *N. crassa* porin, mutants were created which lacked four to six amino acids in some of the proposed β -strand regions of the pore. The electrophysiological and structural properties of the deletion mutants were compared to that of the wild-type protein. Furthermore, regions predicted to be involved in gating were analyzed. Regions were chosen for these studies based on the assumption that, like the *E. coli* OmpF porin, loop regions are responsible for constricting pore size and determining gating properties (Cowan *et al.*, 1992). To determine which amino acid residues participate in the gate of the pore, site-directed mutagenesis was used to create porins with deletions of four to six amino acids in the regions proposed by Popp (1996; Fig. 4.9A) to form the cytoplasmic loops *N. crassa* porin.

4.1. Deletion mutagenesis and cloning into pQE-9

Deletion mutants were generated by making use of the phagemid system (Kunkel *et al.*, 1987) as previously described (section 2.3.1.). The ssDNA obtained was annealed

to each of the deletion mutagenic primers (Table 2.3) and second-strand synthesis was carried out by T7 DNA polymerase. The double-stranded DNA was then transformed into *E. coli* DH5 α and plasmid DNA from potential mutant colonies was sequenced to confirm each of the mutations.

In order to be able to express and purify each of the deletion mutants, a portion of each mutant gene from pBluescript SK⁻ was used to replace the corresponding DNA in His₆porin from the plasmid pQE-9 (Qiagen). In each case, the pBluescript SK⁻ mutant constructs were digested with *Nar*I and *Pst*I to produce 650 bp mutant fragments which were used to replace the corresponding fragment from His₆porin. The resultant pQE-9-derived mutant constructs were then confirmed by DNA sequencing, and introduced into *E. coli* XLI-Blue for protein expression.

4.2. Deletion mutant expression, purification and dialysis

Porin expression was induced by the addition of IPTG to *E. coli* XLI-Blue cells that had been transformed with each of the pQE-9 mutant constructs. Cells were then lysed with urea and the His₆-tagged deletion mutant porins were purified on Ni-NTA agarose as described in section 2.4. The purified deletion mutant porins were eluted from the resin with EDTA in urea and electrophoresed on SDS-PAGE to monitor their purity (Fig 4.1). After confirming the purity of the deletion mutants, protein was diluted either 1:2 or 1:10 with dialysis buffer (section 2.7.), depending on the method of analysis being performed, and subjected to dialysis into Genapol X-80 containing buffer to allow refolding of the protein for biophysical and biochemical analysis.

Of all the deletion mutants expressed in *E. coli* XLI-Blue cells, only

Fig. 4.1. Coomassie Blue stained SDS-PAGE of deletion mutant porins. Lane 1, Low Molecular Weight Marker (Sigma); lane 2, His₆porin ; lane 3, Δ 148-152porin; lane 4, Δ 167-171porin; lane 5, Δ 178-182porin; lane 6, Δ 187-191porin; lane 7, Δ 196-200porin; lane 8, Δ 229-233porin; lane 9, Δ 238-242porin; lane 10, Δ 243-248porin. Each lane was loaded with 2% of the total protein extracted.

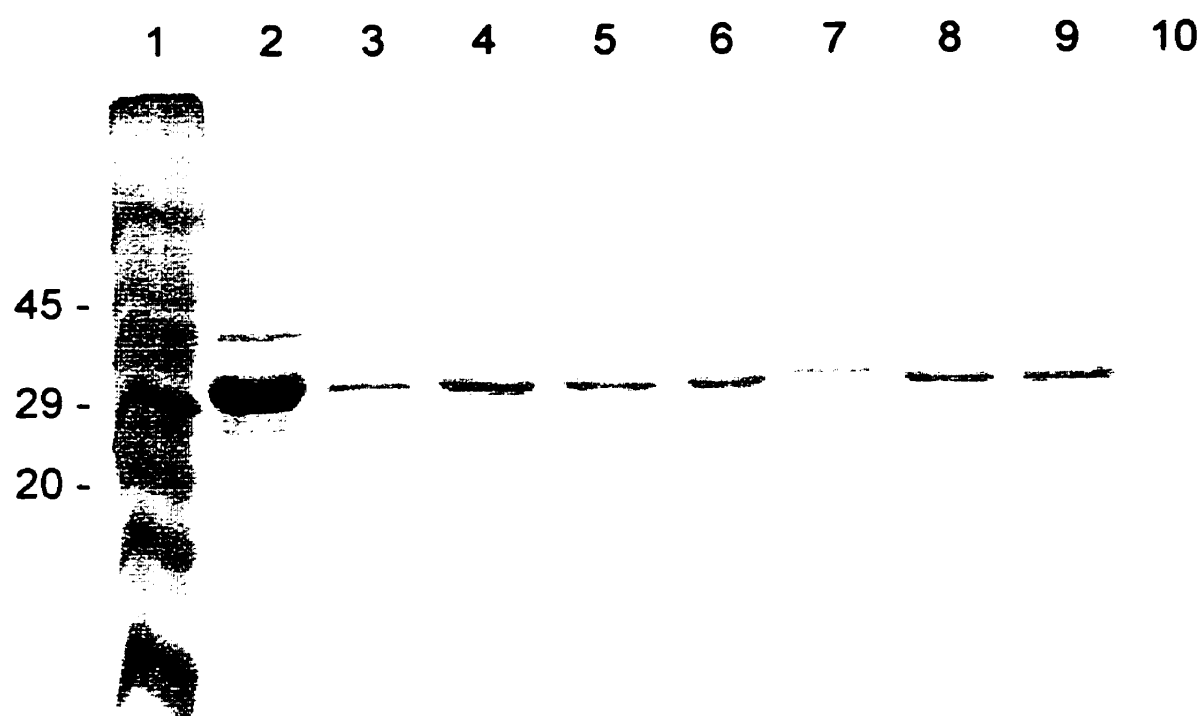
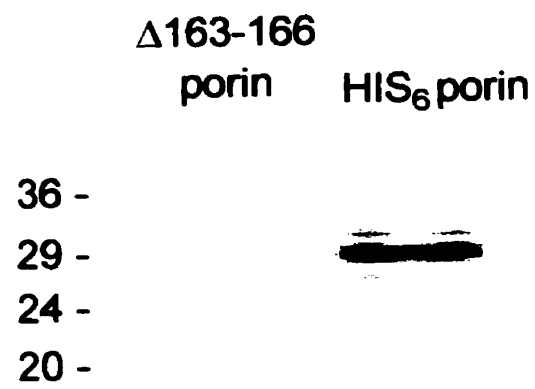


Fig. 4.2. Western blot of $\Delta 163$ -166porin and His₆porin. Each lane of the 12.5% SDS-PAGE gel was loaded with 2% of the total protein extracted. After blotting to nitrocellulose, porin molecules were detected with an antibody directed against the N-terminus of porin. Note the difference in size between $\Delta 163$ -166porin and His₆porin.



$\Delta 163$ -166porin had very weak expression and a truncated protein consistently purified from the Ni-NTA agarose (Fig 4.1). Western blot analysis of this protein with an N-terminal porin antibody revealed that the truncated protein was an amino-terminal fragment of the porin protein (Fig. 4.2). Due to the weak expression of this protein, electrophysiological and CD studies were not done.

4.3. Single channel properties

The electrophysiological properties of each deletion mutant porin were examined and compared to those of wild-type porin to determine if the amino acids deleted in each mutant are critical for these characteristics. Previous studies have shown that the His₆tag does not change the electrophysiological characteristics of porin (Koppel *et al.*, 1998; Popp *et al.*, 1996).

4.3.1. Single channel conductance

The conductance histograms from the single channel readings for each of the deletion mutants are shown in Fig. 4.3 and Fig.4.4. Six mutant porins formed channels that were smaller than His₆porin (Fig. 4.3 and Fig. 4.4). $\Delta 148$ -152porin, $\Delta 178$ -182porin, and $\Delta 187$ -191porin displayed single-channel conductances predominantly between 0.5 nS and 1 nS (Fig. 4.3A, C and D) while $\Delta 167$ -171porin, $\Delta 196$ -200porin and $\Delta 243$ -248porin had conductances between 0.5 nS and 2 nS (Fig. 4.3B and Fig. 4.4A and D). These pores are much smaller than those of His₆porin (Fig. 4.3E). For $\Delta 238$ -242porin, 32% of the conductance steps were found to be between 0.5 and 1 nS while another 32% were found

Fig. 4.3. Histograms of the conductance fluctuations of **(A)** Δ 148-152porin, **(B)** Δ 167-171porin, **(C)** Δ 178-182porin, **(D)** Δ 187-191porin and **(E)** wild-type porin inserted into black lipid bilayers. %G is the frequency that a given conductance increment G is observed in the single channel experiment. %G was calculated by dividing the number of fluctuations with a given conductance increment by the total number of conductance fluctuations. The aqueous phase contained 1 M KCl (pH 6.0). The applied membrane potential was +10 mV; T = 20°C.

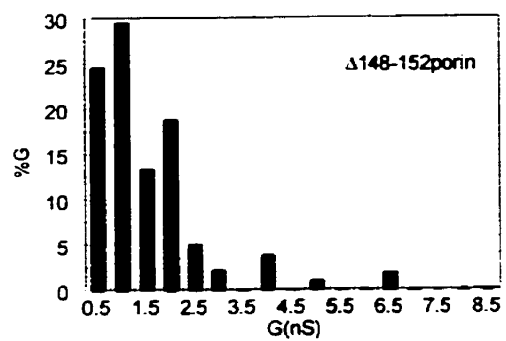
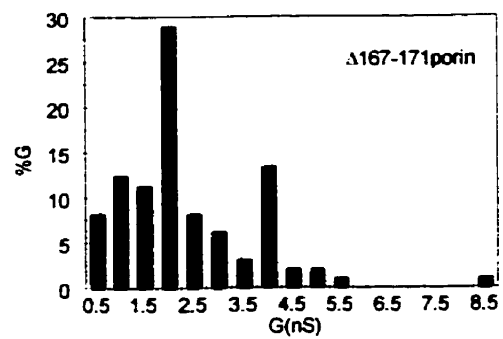
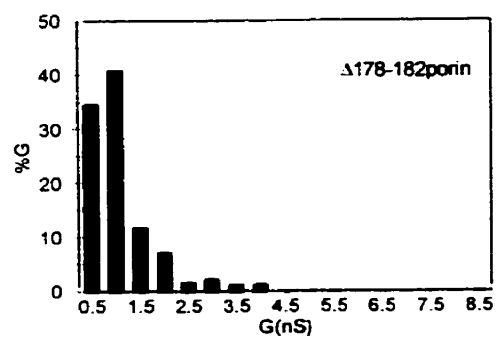
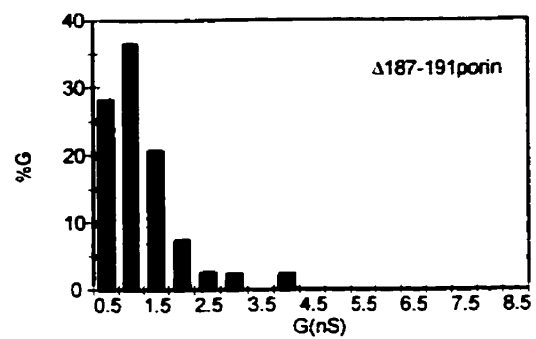
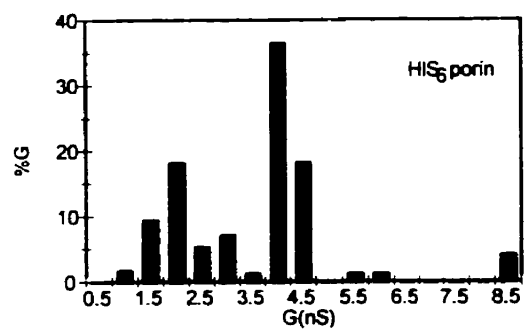
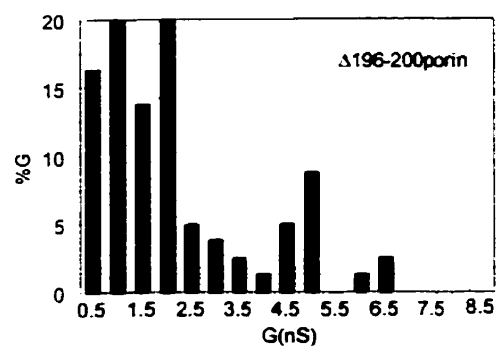
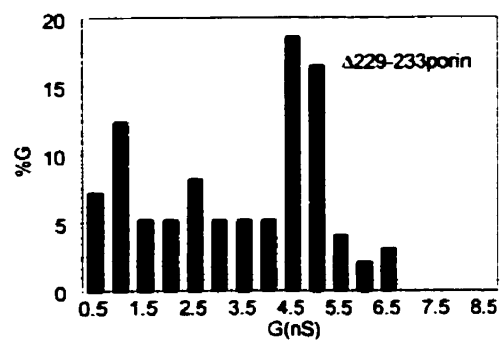
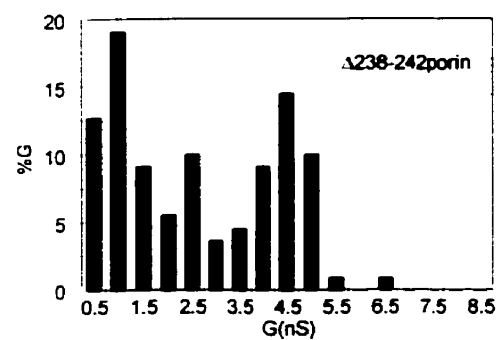
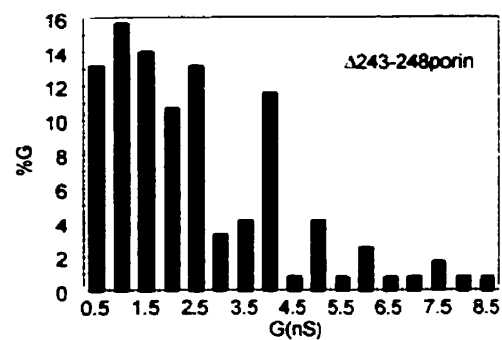
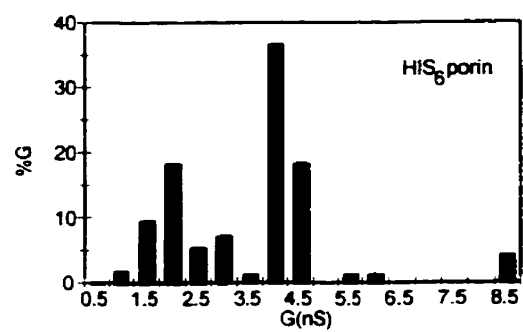
A**B****C****D****E**

Fig 4.4. Histograms of the conductance fluctuations of **(A)** Δ 196-200porin, **(B)** Δ 229-233porin, **(C)** Δ 238-242porin, **(D)** Δ 243-248porin and **(E)** wild-type porin inserted into black lipid bilayers. The experimental conditions are indicated in Fig. 4.3.

A**B****C****D****E**

between 4 nS and 5 nS (Fig 4.4C). This indicates that $\Delta 238-242$ porin forms two different major sets of pores: those pores that are much smaller than His₆porin and those that are similar to it in size (Fig. 4.4). In contrast, $\Delta 229-233$ porin formed stable pores similar in size to those of His₆porin; the majority of the conductance steps were between 4.5 nS and 5 nS (Fig 4.4B).

4.3.2. Voltage-dependent gating

The voltage-dependent gating of each deletion mutant was studied and compared to that of His₆porin. Deletion mutants $\Delta 148-152$ porin, $\Delta 187-191$ porin, $\Delta 229-233$ porin and $\Delta 243-248$ porin displayed conductances that are relatively insensitive to applied voltage (Fig. 4.5A, Fig. 4.6B, Fig. 4.7B and Fig. 4.8B). $\Delta 196-200$ porin was unable to gate at applied voltages above 0 mV, but did display weak gating at applied voltages below 0 mV (Fig. 4.7A). For example, the G_u/G_o at -50 mV for $\Delta 196-200$ porin was 0.69 compared to 0.43 for His₆porin, indicating that conductance of $\Delta 196-200$ porin is less sensitive to the applied voltage than that of His₆porin. $\Delta 178-182$ porin displayed similar gating properties to that of His₆porin at higher applied voltages (Fig. 4.6A). For example, at the applied voltages of -60 mV and 50 mV, the G_u/G_o for $\Delta 178-182$ porin were 0.54 and 0.59 respectively, compared to 0.47 and 0.48 for His₆porin. At the applied voltages of +/- 30 mV however, the G_u/G_o for $\Delta 178-182$ porin were 0.95 and 0.90 respectively, compared to 0.65 and 0.56 for His₆porin, indicating that $\Delta 178-182$ porin is much less sensitive at lower applied voltages. The gating properties of $\Delta 167-171$ porin were unclear due to the limited range of data that could be collected due to pore instability (only to +/-

Fig 4.5. Voltage dependent gating of **(A)** Δ 148-152porin and His₆porin; and **(B)** Δ 167-171porin and His₆porin. The ratio of the conductance, G_u , at a given voltage, U , divided by G_0 at 10 mV is shown as a function of voltage. **(A)** Experiments were repeated between two and four times for Δ 148-152porin; the average G_u/G_0 values are plotted. The data for His₆porin (9) are replotted from Popp *et al.* (1996); vertical lines indicate the standard deviations of the data points. Standard deviations for the Δ 148-152porin data (\square) are all less than 3% of the plotted data and therefore too small to be indicated on the plot. **(B)** Only one experiment was run for Δ 167-171porin (\square). The membranes were formed of DiphPC/*n*-decane. The aqueous phase contained 1 M KCl (pH 6.0); $T = 20^\circ\text{C}$.

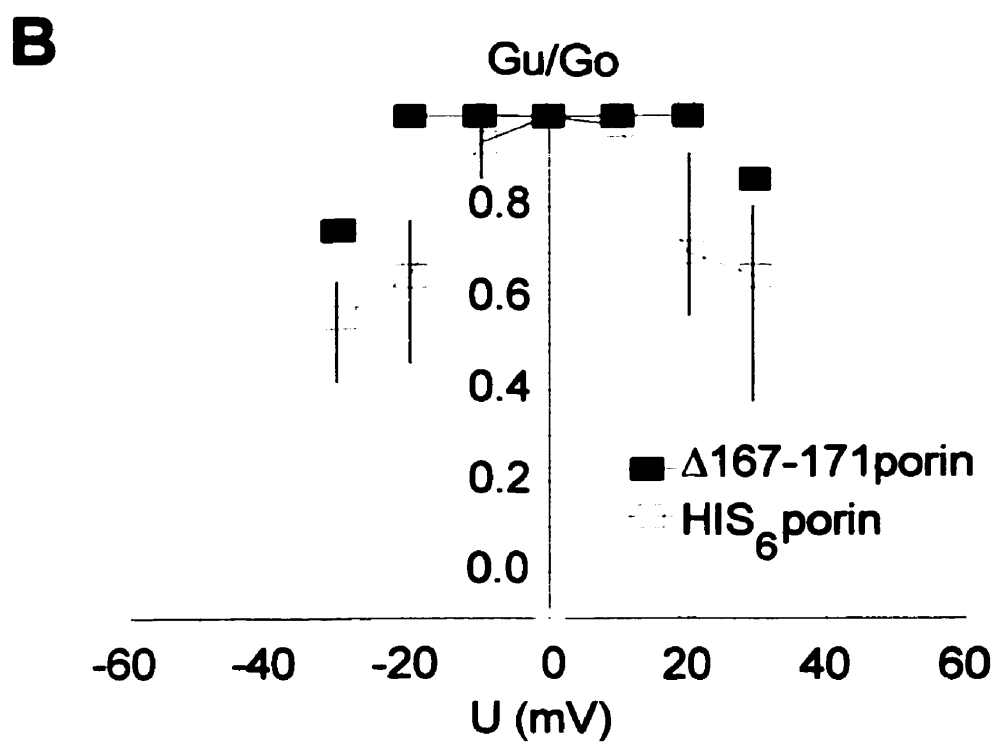
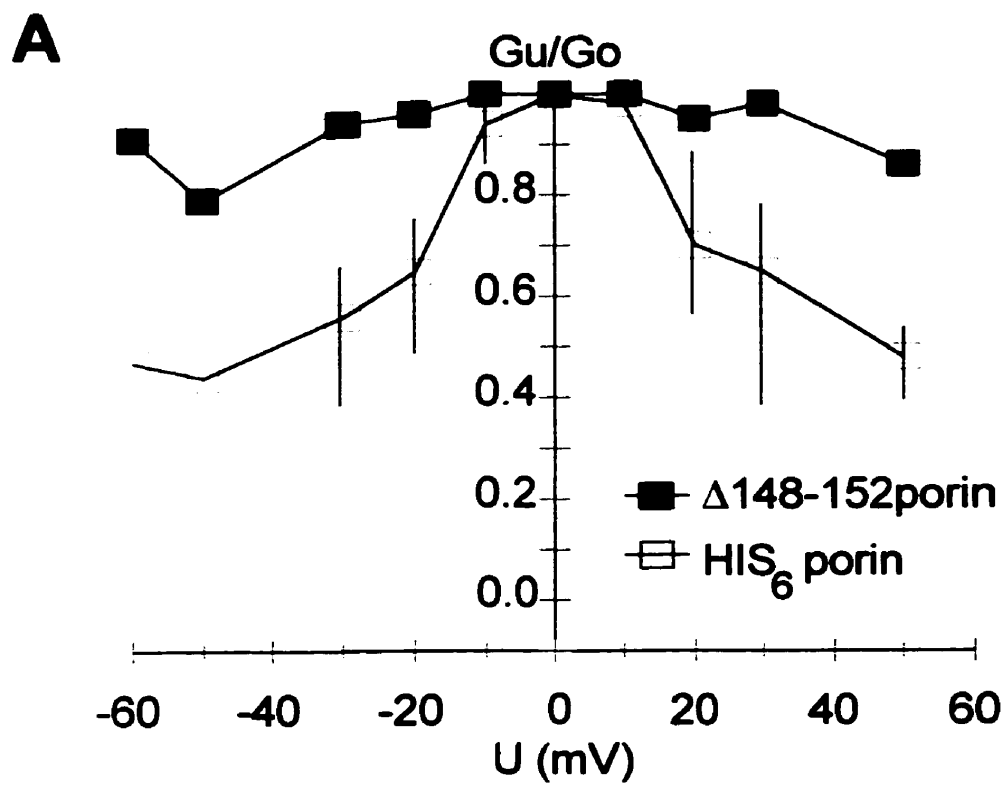


Fig 4.6. Voltage dependent gating of **(A)** $\Delta 178-182$ porin and His₆porin; and **(B)** $\Delta 187-191$ porin and His₆porin. Experiments were carried out and are presented as described in Fig. 4.5.

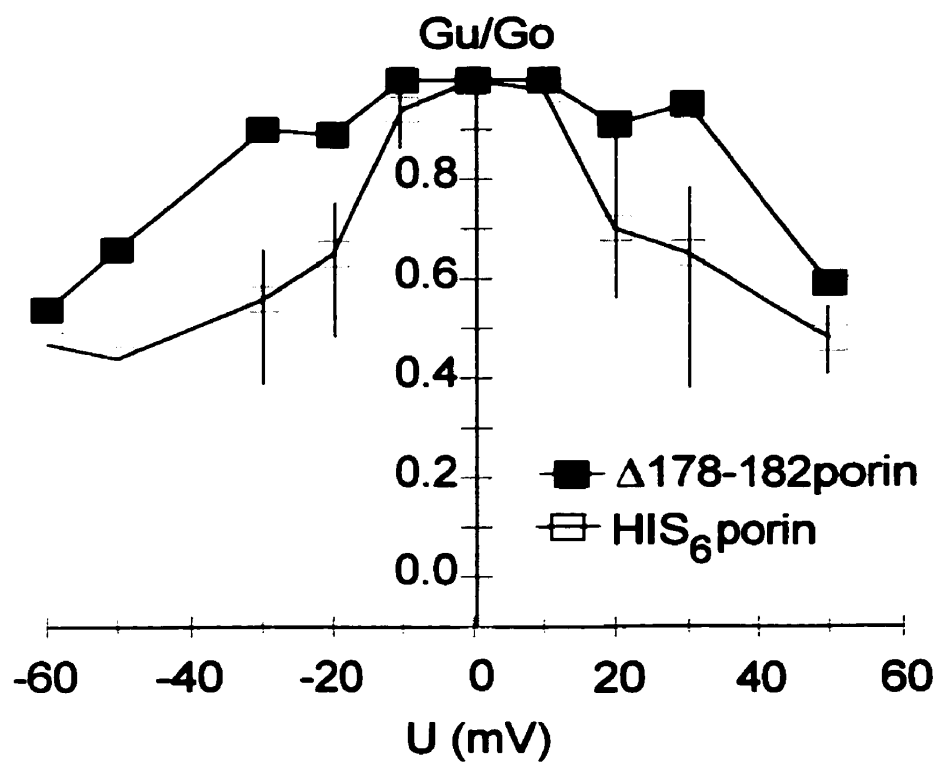
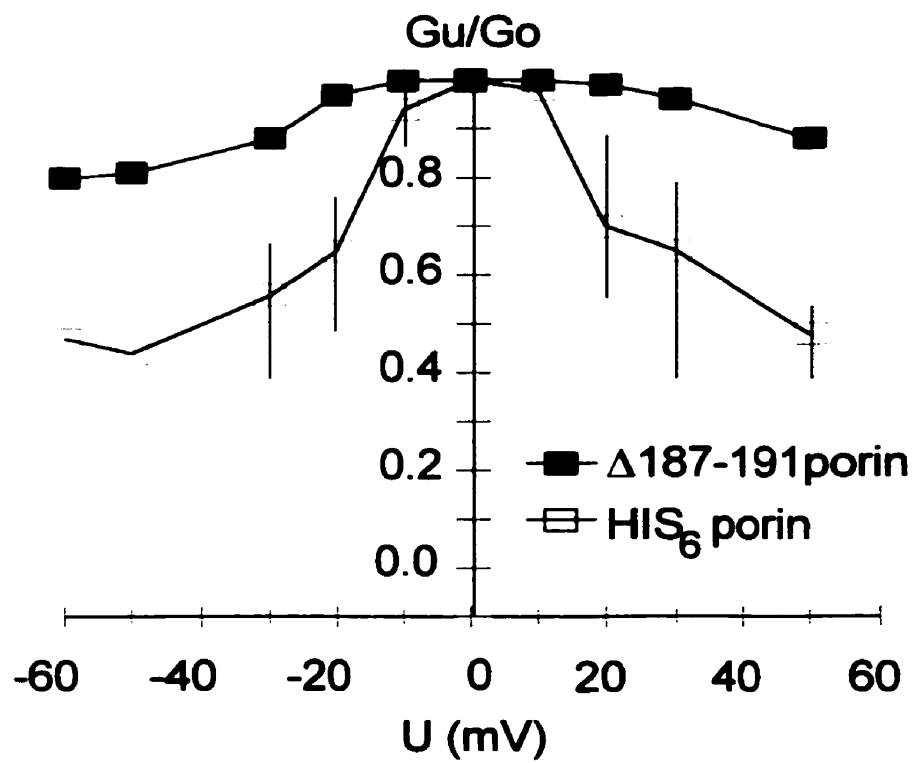
A**B**

Fig 4.7. Voltage dependent gating of **(A)** $\Delta 196$ -200porin and His₆porin; and **(B)** $\Delta 229$ -233porin and His₆porin. Experiments were carried out and are presented as described in Fig. 4.5.

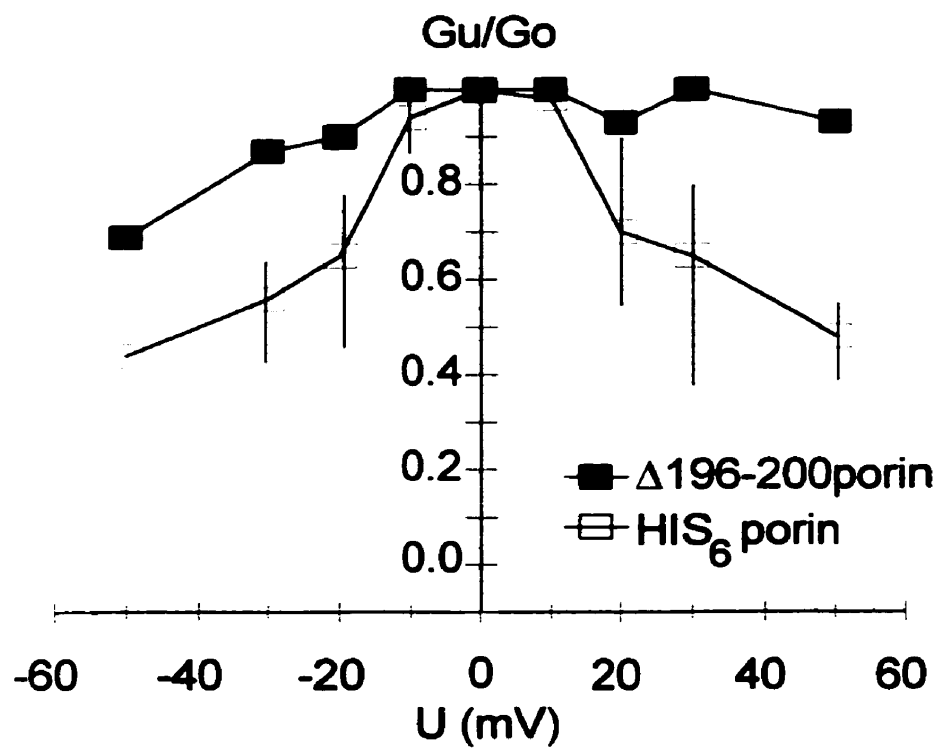
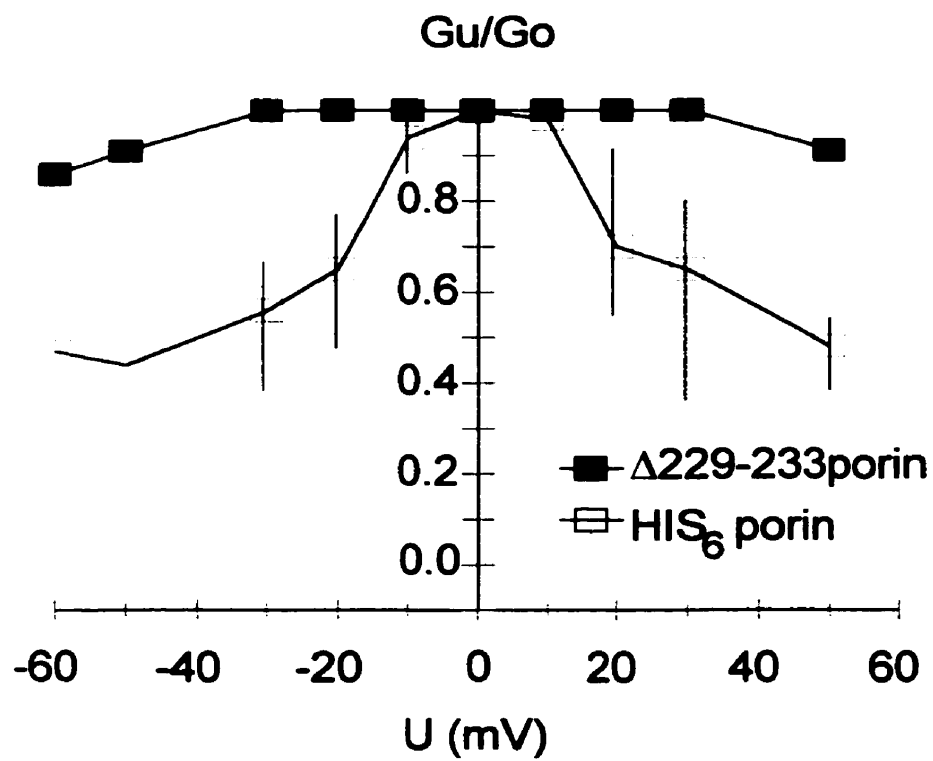
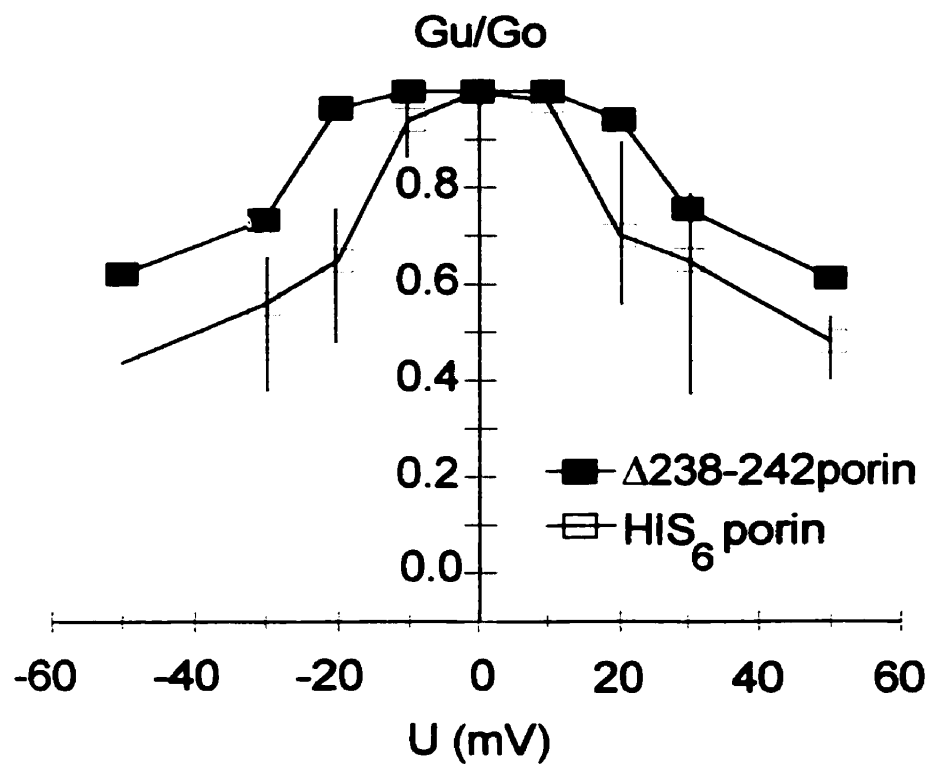
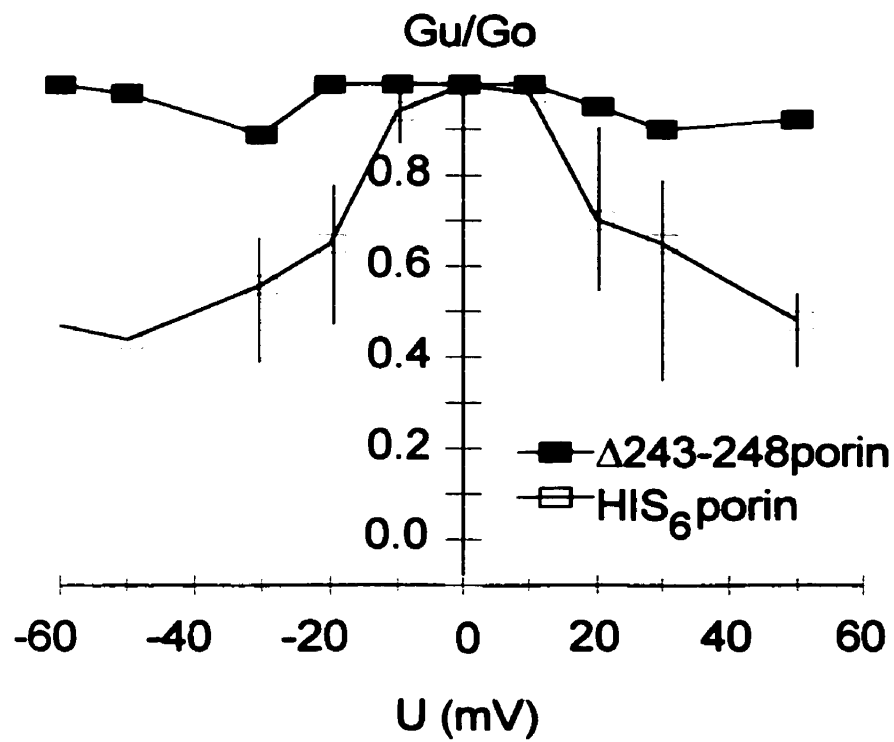
A**B**

Fig. 4.8. Voltage dependent gating of **(A)** $\Delta 238$ -242porin and His₆porin; and **(B)** $\Delta 243$ -248porin and His₆porin. Experiments were carried out and are presented as described in Fig. 4.5.

A**B**

30 mV). The gating of this mutant at +/- 30 mV appeared to be weaker than that of His₆porin (Fig. 4.5B). The Gu/Go of Δ167-171porin at 30 mV was 0.86 compared to 0.65 for His₆porin while at -30 mV the Gu/Go was 0.75 compared to 0.56. The gating of Δ238-242porin was slightly weaker than that of His₆porin (Fig. 4.8A). For example at 50 mV, the Gu/Go of Δ238-242porin was 0.61 compared to 0.48 for His₆porin; however at applied voltages of +/- 20 mV and lower, Δ238-242porin was less sensitive to gating than His₆porin.

4.4. Discussion

Deletions of potential β-strands and loop regions of porin were made to investigate the possible functions of these structural components. β-strands are predicted to be important for pore stability (Seshardi *et al.*, 1998) while the voltage-dependent gate of porin is predicted to be in a loop (Benz, 1994). The electrophysiological properties of each mutant were studied to characterize the different types of mutant porins.

4.4.1. Characterization of deletion mutants

Based on the electrophysiological properties of each deletion mutant, mutants could be placed into four different categories. These four categories included mutants that formed small pores that had no voltage-dependent gating, mutants that formed small pores that displayed weak voltage-dependent gating, mutants that formed normal-sized pores that had no voltage dependent gating, and mutants that formed normal sized pores with normal voltage dependent gating.

The mutants that formed small pores that were not capable of gating included Δ148-152porin, Δ167-171porin and Δ187-191porin (Table 4.1). Δ167-171porin is

Table 4.1. Electrophysiological data obtained from deletion mutant porins.

Porin	Single channel conductance in 1M KCl (nS)	Voltage dependent gating ($G_{-50\text{ mV}}/G_o$)	Reference
Δ 148-152porin	0.5-1.0	0.79, 0.86	this work
Δ 167-171porin	1.0-2.0	0.75, 0.86 ^a	this work
Δ 178-182porin	0.5-1.0	0.66, 0.59	this work
Δ 187-191porin	0.5-1.0	0.81, 0.88	this work
Δ 196-200porin	0.5-2.0	0.69, 0.93	this work
Δ 229-233porin	4.5-5.0	0.91, 0.91	this work
Δ 238-242porin	0.5-1.0, 4.0-5.0	0.623, 0.61	this work
Δ 243-248porin	0.5-2.5, 4.0	0.98, 0.92	this work
Δ N2-12porin	0.5-1.5, 4.0	0.54, 0.60	(Popp <i>et al.</i> , 1996)
Δ C269-283porin	1.5, 3.0	0.42, 0.50	(Popp <i>et al.</i> , 1996)
His ₆ porin	4.0-4.5	0.44, 0.48	(Popp <i>et al.</i> , 1996)

^a at ± 30 mV

included tentatively in this group because the pores were too unstable to allow collection of a sufficient amount of data to determine if this mutant was capable of voltage-dependent gating. The small pores generated by these mutants may indicate that the deleted regions are involved in forming β -strands; hence, their absence results in a smaller barrel. However, due to their lack of voltage-dependent gating, it cannot be ruled out that these regions may also be parts of surface-exposed loops and that the barrel of the pore formed by these mutants is normal but fixed in the closed conformation.

The mutants that formed small pores that displayed weak voltage-dependent gating included $\Delta 178-182$ porin and $\Delta 196-200$ porin (Table 4.1). This group of deleted regions are most likely involved in forming β -strands because there is some gating. However, it is possible that the deleted regions are located in a loop, and that the pores are in a conformation that allows partial closing at relatively high negative potentials.

$\Delta 229-233$ porin and $\Delta 243-248$ porin are mutants that formed normal-sized pores that did not display any voltage-dependent gating (Table 4.1). In the case of $\Delta 243-248$ porin, the pores varied in size, but there was still a reasonable number of pores of a normal size (4 nS). Therefore, the corresponding segments are most likely part of surface-exposed loops due to the fact that proteins lacking them form normal-sized pores. The lack of voltage-dependent gating indicates that these segments are also directly, or indirectly, involved in voltage-dependent gating.

$\Delta 238-242$ porin is the mutant that formed normal-sized pores with normal voltage-dependent gating (Table 4.1). This indicates that this region is most likely part of a surface-exposed loop that is not involved in voltage-dependent gating.

Fig. 4.9. The current structural models of *N. crassa* mitochondrial porin including (A) the 16-stranded β -barrel model of Popp (1996) and (B) the 13-stranded β -barrel model of Song *et al.* (1998b).

A
 F
 H
 S
 N
 T
 P
 H
 K
 T
 V
 F
 V
 N
 H
 D
 K
 V
 T
 S
 G
 L
 E
 K
 F
 T
 O
 K
 P
 N
 T
 W
 Q
 V
 T
 L
 G
 N
 T
 A
 N
 A
 L
 E
 T
 V
 E
 M
 A
 N
 L
 A
 P
 L
 F
 S
 I
 G
 N
 L
 G
 K
 N
 L
 F
 K
 Q
 S
 N
 L
 F
 A
 R
 G
 K
 F
 N
 L
 F
 L
 D
 F
 A
 R
 G
 H
 F
 Q
 P
 T
 A
 N
 D
 A
 I
 V
 D
 H
 E
 G
 S
 Y
 Q
 T
 I
 A
 K
 Q
 V
 D
 Y
 A
 V
 G
 Y
 H
 A
 P
 T
 Y
 S
 A
 I
 T
 A
 T
 D
 N
 V
 N
 K
 H
 Y
 Y
 S
 A
 F
 S
 V
 L
 S
 Q
 V
 E
 A
 G
 S
 A
 T
 W
 N
 S
 K
 T
 G
 N
 P
 D
 I
 R
 Y
 K
 T
 A
 V
 E
 L
 G
 V
 T
 O
 K
 L
 N
 I
 K
 G
 K
 V
 F
 S
 V
 P
 D
 I
 R
 Y
 G
 V
 A
 I
 A
 Y
 N
 V
 L
 L
 E
 G
 D
 R
 V
 A
 I
 A
 Y
 N
 V
 L
 L
 E
 G
 200

5
 K112
 A G R A N T A P L F S H G A F D L L K
 F N L H F K Q S N F G I A D I N A G Y V A A K Q
 A S Y Y H K V N S Q V E A G S K A T W
 3180
 F V S L N D P V S F V K I N D
 K T A V E L G V T N G T K 3211
 E G
 L V N Y A I A V G
 S
 F T F S T G V K H T A
 D Q
 M A V P A N V D T F K G E L A G S V
 - - - - -
 D S7 F A N P T N S K V E I T G
 S K A I A L D H23 A
 K N L F L A
 Y - -
 135
 P
 0158
 V
 I A A K Q
 T
 G Y S A A V
 224
 G
 2202
 S
 F T F S T G V K H T A
 D Q

Table 4.2. Hydropathic values assigned to residues in constructing Kyte and Doolittle plots (1982).

Amino Acid	Hydropathicity
A	1.8
R	-4.5
N	-3.5
D	-3.5
C	2.5
E	-3.5
Q	-3.5
G	-0.4
H	-3.2
I	4.5
L	3.8
K	-3.9
M	1.9
F	2.8
P	-1.6
S	-0.8
T	-0.7
W	-0.9
Y	-1.3
V	4.2

4.4.2. Implications to structural models of porin

In this study, the deletions made in β -strands and surface-exposed loops were selected based on the 16-stranded β -barrel model (Fig. 4.9A) described by Popp (1996). Based on the results of the mutant porins described in this study, two new structural models of *N. crassa* mitochondrial porin can be proposed; the current data set does not exclude either model. Kyte and Doolittle hydropathic plots, which calculate average hydrophobicity of protein segments based on the actual hydrophobic values of each amino acid (Kyte and Doolittle, 1982; Table 4.2), were made of *N. crassa* mitochondrial porin and each mutant variant to help construct both models. The hydrophobic properties of the known *E. coli* OmpF porin, whose X-ray crystal structure was resolved by Cowan *et al.* (1992) was used to interpret the hydropathy data.

4.4.2.1. Model 1

The first structural model being proposed is a 16-stranded β -barrel (Fig. 4.10) that is a variation of the Popp model (see 1.4.2.4.; Fig. 4.9A). This structural model varies from the Popp-model only in the C-terminal half of porin, where the deleted regions made in this study are located. The similarities and differences between model 1, the Popp model and the 13-stranded β -barrel model (Fig. 4.9B) by Song *et al.* (1998b; see 1.3.2.) are also discussed.

In model 1, the residues deleted in $\Delta 148-152$ porin are all placed in β -strand 10 (Fig. 4.10), just as they are in the Popp model (Fig. 4.9A). The 13-stranded model by Song *et al.* (1998b) also places these residues in a β -strand, β -strand 8 (Fig. 4.9B). This mutant formed pores that were small and unable to gate. This region is hydrophobic

Fig. 4.10. The newly proposed 16-stranded β -barrel model, model 1. The residues deleted from the different deletion mutants are indicated in bold font. Boxed residues are predicted to be in membrane-spanning β -strands. Amino acid residues are numbered, starting with the N-terminus.

CYTOSOL

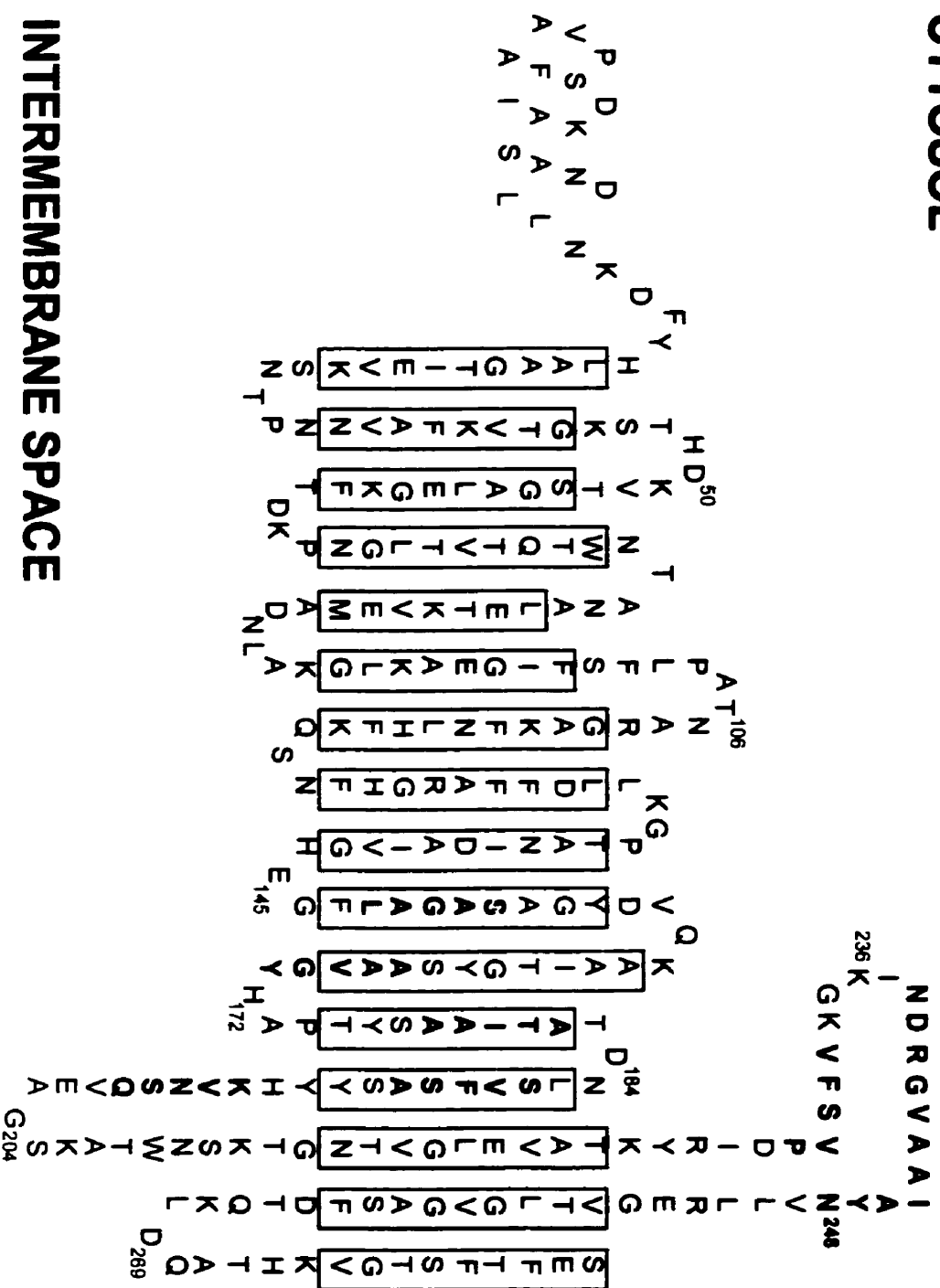


Table 4.3. Values from the Kyte and Doolittle (1982) hydropathic plot of *N. crassa* mitochondrial porin.

Amino Acid ^a (Residue Number): Score ^b					
V(3): 1.62	P(4): 1.80	A(5): 1.28	F(6): -0.26	S(7): 0.96	D(8): 0.96
I(9): -0.38	A(10): -0.38	K(11): 0.68	S(12): -0.92	A(13): -1.98	N(14): -0.44
D(15): 0.48	L(16): -0.58	L(17): -0.66	N(18): -0.66	K(19): -0.86	D(20): -1.88
F(21): -1.82	Y(22): -0.28	H(23): 0.78	L(24): 0.58	A(25): 0.76	A(26): 1.26
G(27): 1.40	T(28): 0.34	I(29): 0.82	E(30): 0.12	V(31): 0.10	K(32): -1.50
S(33): -0.94	N(34): -2.10	T(35): -2.02	P(36): -2.56	N(37): -1.02	N(38): -0.52
V(39): 0.36	A(40): 0.28	F(41): 1.82	K(42): 0.84	V(43): 0.40	T(44): -0.94
G(45): -0.32	K(46): -1.30	S(47): -1.80	T(48): -2.42	H(49): -2.42	D(50): -1.42
K(51): -1.42	V(52): -0.94	T(53): -0.32	S(54): 0.82	G(55): 0.74	A(56): 0.18
L(57): 0.26	E(58): -0.44	G(59): -0.24	K(60): -1.14	F(61): -1.14	T(62): -1.84
D(63): -1.38	K(64): -2.64	P(65): -2.58	N(66): -1.12	G(67): -0.48	L(68): 0.68
T(69): 1.24	V(70): 0.62	T(71): -0.28	Q(72): -0.32	T(73): -1.86	W(74): -1.14
N(75): -0.80	T(76): -1.36	A(77): -0.82	N(78): 0.64	A(79): 0.08	L(80): -0.42
E(81): -0.50	T(82): -0.02	K(83): -1.48	V(84): -0.40	E(85): 0.10	M(86): 0.18
A(87): -1.36	D(88): 0.10	N(89): 0.08	L(90): -1.06	A(91): -0.44	K(92): 1.02
G(93): -0.52	L(94): -0.52	K(95): -0.44	A(96): -0.44	E(97): -0.30	G(98): 1.04
I(99): 1.78	F(100): 1.78	S(101): 2.62	F(102): 1.40	L(103): 1.20	P(104): 1.22
A(105): -0.04	T(106): -0.44	N(107): -1.02	A(108): -1.46	R(109): -0.96	G(110): -1.04
A(111): -0.84	K(112): -0.64	F(113): 0.20	N(114): -0.80	L(115): 0.54	H(116): -0.80
F(117): -0.80	K(118): -1.72	Q(119): -1.78	S(120): -1.78	N(121): -1.64	F(122): -1.02
H(123): -1.76	G(124): -0.70	R(125): -0.70	A(126): 0.50	F(127): -1.20	F(128): 1.54
D(129): 1.94	L(130): 0.60	L(131): -0.04	K(132): 0.34	G(133): -0.56	P(134): -0.96
T(135): -0.88	A(136): 0.10	N(137): -0.28	I(138): 0.22	D(139): 0.76	A(140): 2.30
I(141): 1.32	V(142): 1.38	G(143): 0.32	H(144): -0.66	E(145): -0.94	G(146): -0.10
F(147): 0.90	L(148): 1.52	A(149): 1.96	G(150): 1.24	A(151): 0.84	S(152): 0.40
A(153): 0.22	G(154): -0.84	Y(155): 0.16	D(156): -0.90	V(157): -1.60	Q(158): -0.98
K(159): 0.08	A(160): 0.14	A(161): 0.70	I(162): 1.40	T(163): 0.78	G(164): 0.26
Y(165): -0.28	S(166): 0.22	A(167): 1.14	A(168): 1.32	V(169): 1.22	G(170): 0.22

Y(171): 0.22	H(172): -0.94	A(173): -1.00	P(174): -1.00	T(175): -0.52	Y(176): -0.52
S(177): 0.16	A(178): 1.20	A(179): 1.32	I(180): 1.84	T(181): 1.34	A(182): 0.28
T(183): -1.32	D(184): -0.42	N(185): -0.94	L(186): 0.04	S(187): 1.30	V(188): 1.84
F(189): 1.44	S(190): 1.44	A(191): 0.34	S(192): -0.48	Y(193): -0.96	Y(194): -2.10
H(195): -1.10	K(196): -1.54	V(197): -1.44	N(198): -1.50	S(199): 0.12	Q(200): -1.42
V(201): -0.36	E(202): -0.28	A(203): 0.26	G(204): -1.36	S(205): -0.30	K(206): -0.80
A(207): -0.90	T(208): -1.44	W(209): -0.82	N(210): -1.96	S(211): -1.96	K(212): -1.86
T(213): -1.86	G(214): -1.84	N(215): -0.22	T(216): -0.16	V(217): 0.68	G(218): 0.68
L(219): 1.66	E(220): 1.18	V(221): 1.12	A(222): -0.42	T(223): 0.02	K(224): -1.72
Y(225): -1.18	R(226): -1.74	I(227): -1.28	D(228): -0.18	P(229): 0.56	V(230): 0.22
S(231): 1.76	F(232): 1.30	V(233): 0.38	K(234): -0.24	G(235): 0.10	K(236): -1.44
I(237): -1.36	N(238): -2.18	D(239): -1.48	R(240): -1.54	G(241): -0.48	V(242): 0.58
A(243): 2.38	A(244): 2.82	I(245): 1.72	A(246): 0.66	Y(247): 1.14	N(248): 1.00
V(249): 1.40	L(250): 0.76	L(251): 0.76	R(252): -0.16	E(253): -0.08	G(254): -0.98
V(255): 0.68	T(256): 1.30	L(257): 2.22	G(258): 1.30	V(259): 1.80	G(260): 0.88
A(261): 1.52	S(262): -0.02	F(263): -0.08	D(264): -1.14	T(265): -1.76	Q(266): -1.56
K(267): -1.56	L(268): -2.12	D(269): -1.06	Q(270): -0.42	A(271): -1.82	T(272): -1.90
H(273): -0.36	K(274): -0.80	V(275): -0.80	G(276): -0.32	T(277): 1.02	S(278): 0.04
F(279): 0.68	T(280): 0.12	F(281): 0.12			

^a single letter amino acid code

^b measured over a window size of 5 amino acids

(Table 4.3), indicating that it could be in a membrane spanning β -strand, which is consistent with the hydrophobic properties of the OmpF porin structure (Cowan *et al.*, 1992). In the current model, β -strand 10 is flanked by a three residue turn (residues 144-146) in the intermembrane space and a four residue cytoplasmic-exposed loop (residues 156-159). Deleting the segment of 148-152, which is hydrophobic, could cause some of the residues in the three residue turn or the four residue loop to move into β -strand 10 to replace the deleted residues. In $\Delta 148-152$ porin, residues 153-156 are still in a weakly hydrophobic environment (Table 4.4). However, residues 145-147 and residues 157-159, some of which would be required to move into the membrane, are in hydrophilic regions of the protein (Table 4.4). This may form a less stable β -strand 10 which could cause the protein to misfold, such that a channel with fewer transmembrane segments is formed, resulting in a pore with a smaller conductance. In this case, the gate might be unable to interact with the pore, thereby preventing voltage-dependent gating.

Like $\Delta 148-152$ porin, $\Delta 167-171$ porin formed pores that were small in size that were tentatively classified as being not able to gate. Based on these results, residues 167-169 were placed in a new β -strand 11 (Fig. 4.10), instead of the surface-exposed loop that connects β -strands 10 and 11 as in the Popp model (Fig 4.9A) or in an intermembrane space loop as proposed by Song *et al.* (1998b; Fig. 4.9B). Residues 167-169 (Table 4.3) are quite hydrophobic similar to residues 148-152, which provides some support that these residues could be placed in a β -strand. Residues 170 and 171, which are only in a slightly hydrophobic environment (Table 4.3), are placed in a β -turn in the intermembrane space

Table 4.4. Kyte and Doolittle plots of the newly formed segments formed in each of the deletions mutants (Kyte and Doolittle, 1982).

Deletion	Hydropathicity of newly formed segment
$\Delta 148-152$ porin	H144, E145, G146, F147, A153, G154, Y155, D156, V157, Q158, K159 0.32, -0.66, -0.94, -0.50, 0.06, 0.50, -0.12, 0.16, -0.90, -1.60, -0.98
$\Delta 167-171$ porin	T163, G164, Y165, S166, H172, A173, P174, T175 1.40, 0.78, 0.26, -1.28, -0.78, -1.02, -0.90, -1.00
$\Delta 178-182$ porin	P174, T175, Y176, S177, T183, D184, N185, L186 -1.00, -1.00, -0.52, -1.02, -1.40, -1.96, -0.94, -0.94
$\Delta 187-191$ porin	T183, D184, N185, L186, S192, Y193, Y194, H195 0.28, -1.32, -0.42, -0.94, -1.06, -0.62, -0.56, -2.10
$\Delta 196-200$ porin	S192, Y193, Y194, H195, V201, E202, A203, G204 0.34, -0.48, -0.96, -0.48, -1.02, -0.40, -0.22, 0.26
$\Delta 229-233$ porin	Y225, R226, I227, D228, K234, G235, K236, I237 -1.72, -1.18, -1.74, -1.74, -1.56, -1.44, -1.44, -1.44
$\Delta 238-242$ porin	K234, G235, K236, I237, A243, A244, I245, A246 0.38, -0.24, 0.10, -0.38, 0.76, 1.74, 2.88, 1.72
$\Delta 243-248$ porin	D239, R240, G241, V242, V249, I250, L251, R252 -2.18, -1.48, -1.54, 0.00, 1.46, 3.12, 2.30, 0.76

(Fig. 4.10).

$\Delta 187-191$ porin also formed small pores that did not display any voltage-dependent gating. Like $\Delta 148-152$ porin, where all five deleted residues were placed into β -strand 10, residues 187-191 have been placed into β -strand 13 in model 1 (Fig. 4.10) based on the same arguments. This agrees with the Popp model, which places these residues in β -strand 12, but disagrees with the Song *et al.* model that places these residues in a surface-exposed loop. The difference in strand location between the Popp model and model 1 is due to the new β -strand in model 1 that includes residues 167-169. $\Delta 187-191$ porin may form small pores that cannot gate because the five deleted residues are in a hydrophobic region (Table 4.3) while the possible replacement residues for β -strand 13 are hydrophilic (Table 4.4), suggesting that they are poor replacements. This could lead to protein misfolding and the formation of a channel with fewer transmembrane segments and altered voltage-dependent gating.

$\Delta 178-182$ porin formed small pores that displayed weak voltage-dependent gating. Residues 178-182 have been placed into a β -strand (12) in model 1 (Fig 4.10), as they are in the Popp (1996) and Song *et al.* (1998b) models, which also place these residues into β -strands (Fig 4.9). The five residues are all hydrophobic in nature (Table 4.3), which supports their placement into membrane spanning β -strands. It is not clear why $\Delta 178-182$ porin displays some voltage-dependent gating, because all the possible replacements for the deleted segment are all hydrophilic (Table 4.4). This suggests that the newly formed β -strand should be unstable like the three previously discussed mutants. One

explanation may be that this β -strand is slightly more tolerant to hydrophilic replacements such that the degree of misfolding is less and the gate is able to interact with the misfolded pores.

Δ 196-200porin formed pores that ranged in size between 0.5-2.0 nS, with a few normal-sized pores that displayed weak gating at negative potentials. This suggests that residues 196-200 may be involved in a loop rather than a β -strand and that residues 196-200 may be indirectly involved with the gating process. Model 1 places residues 196-200 in an intermembrane space loop that connects β -strands 13 and 14 (Fig 4.10), while both the Popp model and the Song model place these residues in surface-exposed loops. Another notable difference between the Popp model and model 1, is that model 1 places β -strand 13 from the Popp model (Fig. 9A) into the intermembrane space loop (Fig 4.10) to make room for the newly formed β -strand 11 (see above). The criterion used for model 1 is the hydrophilic nature of residues 196-200 (Table 4.2), which supports their placement into a loop region.

The deletion mutants Δ 229-233porin and Δ 243-248porin were both able to form normal-sized pores that displayed no voltage-dependent gating. These results suggest that residues 229-233 and 243-248 are not required for the formation of a normal pore, but are involved in the gating process. Therefore, they are placed in a loop in model 1, in agreement with the Popp model that also places these residues in a surface-exposed loop (connecting β -strands 13 and 14; Figs. 4.9A and 4.10). In contrast, the Song model places these residues in two different β -strands (Fig. 4.9B). Residues 229-233 and 243-248 are hydrophobic (Table 4.3), with residues 243-245 found in the most hydrophobic part of

porin. Since the channel formed by porin is water-filled, and as charged residues have been found to act as voltage sensors (Thomas *et al.*, 1993), it is unclear what role these segments have in the gating process. One possibility is that these segments are required to physically move the gate into contact with the pore.

$\Delta 238-242$ porin formed normal-sized pores which gated normally. This suggests that residues 238-242 are not required for the formation of a normal channel and that they are not involved in the gating process. Therefore, model 1 places this segment in a surface-exposed loop that connects β -strands 13 and 14, which is in agreement with the Popp model (Figs. 4.9A and 4.10).

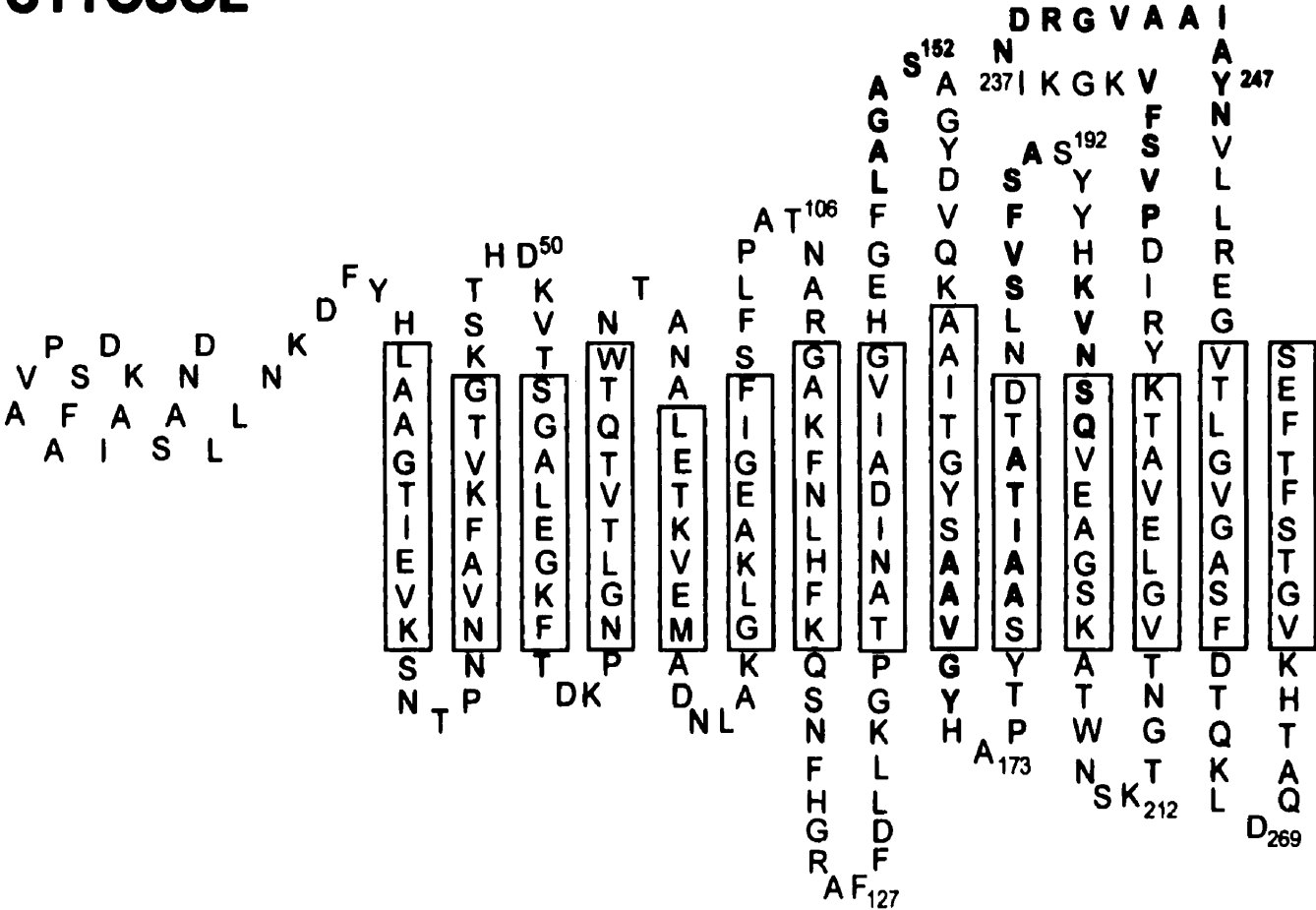
The last two β -strands proposed in the Popp model and the Song *et al.* model contain the same amino acid residues (Fig. 4.9) and are not changed in model 1. A previously made deletion mutant, $\Delta C269-283$ porin (Popp *et al.*, 1996), formed small pores that displayed normal voltage-dependent gating indicating that the residues most likely are located in a β -strand. However, in this case, the deletion of a β -strand does not affect stability of the structure or gating to a very large extent.

4.4.2.2. Model 2

The data obtained in these studies is consistent with a second model for porin structure, model 2. This second structural model is a 14-stranded β -barrel (Fig 4.11). Model 2 is another variation of the Popp model and is exactly the same as the Popp model and model 1 up to β -strand 7, after which model 2 deviates significantly. The orientation of the long loops in model 2 were also taken into consideration in constructing this model so that most of the loops face the external side of the membrane rather than the

Fig. 4.11. The newly proposed 14-stranded β -barrel model, model 2. The residues are labelled as in Fig. 4.10.

CYTOSOL



intermembrane space. The similarities and differences between model 2, model 1, the Popp model and the Song *et al.* model are discussed below.

The residues deleted to create mutants $\Delta 148-152$ porin and $\Delta 187-191$ porin were placed in two different β -strands in model 1 and the Popp model (Figs. 4.9A and 4.10) but are placed in two different surface-exposed loops in model 2. Residues 148-152 are placed in a β -strand in the Song *et al.* model while residues 187-191, as in model 2, are placed in a surface-exposed loop (Fig 4.9B). $\Delta 148-152$ porin and $\Delta 187-191$ porin formed small pores that did not display voltage-dependent gating which, as for model 1, could be explained by protein misfolding (see 4.4.2.1.). In model 2, it is proposed that residues 148-152 and 187-191 are in loops that may be needed to allow opening of the gate. A loss of residues in either of these loops may trap porin in a closed state, where it can no longer gate resulting in a pore with an apparent decreased pore size. To accommodate the placement of residues 148-152 and 187-191 into surface-exposed loops, residues composing β -strand 8 (residues 122-130) in model 1 and the Popp model are placed into a loop that sits in the intermembrane space (Fig. 4.11). The placement of residues 122-130 into a loop also disagrees with the Song *et al.* model (Fig. 4.9B). Residues 123-125 and 129 are hydrophilic (Table 4.3), while residues 126 and 128-130 are hydrophobic, suggesting that these residues could be in a loop or a β -strand.

Model 2, like model 1, places residues 167-169 into a β -strand, while residues 170-171 are placed in a short loop that faces the intermembrane space (Figs. 4.10 and 4.11), based on the same arguments used for model 1 (see 4.4.2.1.). The models by Popp and Song *et al.* placed all of these residues in loops (Fig. 4.9).

Δ 178-182porin formed small pores that displayed weak voltage-dependent gating. Based on the same arguments used for model 1 (see 4.4.2.1.), model 2 places residues 178-182 into a β -strand (Figs. 4.9, 4.10 and 4.11), which is consistent with all models under discussion.

Most of the channels formed by Δ 196-200porin were smaller than normal pores and usually displayed weak voltage-dependent gating at negative potentials. Unlike model 1, and the models of Popp (1996) and Song *et al.* (1998b) which placed residues 196-200 into loop regions (Figs. 4.9 and 4.10), model 2 places residues 196-198 into a loop and residues 199 and 200 into a β -strand (Fig 4.11). Since Δ 196-200porin was also able to form normal-sized pores (Fig. 4.4A) that displayed some weak gating, it is difficult to determine where these five deleted residues should be placed. Table 4.3 shows that residues 196-198 and 200 are in a hydrophilic segment while residue 199 is in a hydrophobic segment, which would indicate that these residues have a greater chance of being located in a loop. To maintain loops on the external face of the membrane, a β -strand is needed in an area of porin where mainly hydrophilic residues predominate (Table 4.3) and since residue 199 is hydrophobic in nature, it seems like a good candidate to be included in a β -strand that includes residues 199-206. Some of the other residues involved in this β -strand are residues from the Popp model β -strand 13 (Fig. 4.9A), but all the residues making up this strand are found in loops in model 1 and the Song *et al.* (1998) model (Figs. 4.9B and 4.10).

The last 3 β -strands in each of model 1, model 2 and the Popp model are basically made up by the same amino acids (Figs. 4.9A, 4.10 and 4.11). Connecting the first two of

these three β -strands is a large loop which includes the residues deleted from the mutants $\Delta 229-233$ porin, $\Delta 238-242$ porin and $\Delta 243-248$ porin. Song *et al.* placed residues 229-233 and 243-248 into β -strands, but since these mutants all can form normal sized pores, it is more likely that they are found in a loop and involved with voltage-dependent gating as previously mentioned (see 4.4.2.1.).

4.5. Summary

The deletion mutants made in this study could be classified into four different categories, based on the electrophysiological characteristics of each mutant. Based on these mutants, two new structural models were constructed of *N. crassa* mitochondrial porin. Model 1 is a 16-stranded β -barrel, while model 2 is a 14-stranded β -barrel. The construction of model 1 and model 2 in this study, as well as the Popp (1996) model and the Song *et al.* (1998b) model, rely on relatively low resolution methods for predicting protein structure. Therefore, further experimental work is required in order to determine which model most closely predicts the secondary structure of *N. crassa* mitochondrial porin. Experiments involving the binding of antibodies to porin slightly agree (Stanley *et al.*, 1995) more with model 1 over model 2. However, overall the results are not consistent with either model. Based on all the results obtained, model 1 is slightly favoured over model 2.

4.6. Future Work

Possibilities for further work could include more deletion mutagenesis or protease cleavage of porin in intact mitochondria. Protease cleavage could help determine the residues that are found in surface-exposed loops. Circular dichroism studies of each

mutant could detect differences in secondary structure. The most reliable way to confirm or reject any of these models is to obtain a 3-dimensional structure of *N. crassa* mitochondrial porin by NMR or X-ray crystallography.

References

- Bainbridge, G., Armstrong, G. A., Dover, L. G., Whelan, K. F., and Lakey, J. H. (1998a). Displacement of OmpF loop 3 is not required for the membrane translocation of colicins N and A in vivo. *FEBS Lett.* 432, 117-122.
- Bainbridge, G., Mobasheri, H., Armstrong, G. A., Lea, E. J. A., and Lakey, J. H. (1998b). Voltage-gating of *Escherichia coli* porin: A Cystine-scanning mutagenesis study of Loop 3. *J. Mol. Biol.* 275, 71-176.
- Bathori, G., Parolini, I., Tombola, F., Szabo, I., Messina, A., Oliva, M., De Pinto, V., Lisanti, M., Sargiacomo, M., and Zoratti, M. (1999). Porin is present in the plasma membrane where it is concentrated in caveolae and caveolae-related domains. *J. Biol. Chem.* 274, 29607-29612.
- Benz, R. (1994). Permeation of hydrophilic solutes through mitochondrial outer membranes: review on mitochondrial porins. *Biochim. Biophys. Acta* 1197, 167-196.
- Benz, R., Jenko, K., Boos, W., and Lauger, P. (1978). Formation of large, ion-permeable membrane channels by the matrix protein (porin) of *Escherichia coli*. *Biochim. Biophys. Acta* 511, 305-319.
- Berrier, C., Besnard, M., and Ghazi, A. (1997). Electrophysiological characteristics of the PhoE porin channel from *Escherichia coli*. Implications for the possible existence of a superfamily of ion channels. *J. Membrane Biol.* 156, 105-115.
- Blachly-Dyson, E., Baldini, A., Litt, M., McCabe, E. R., and Forte, M. (1994). Human genes encoding the voltage-dependent anion channel (VDAC) of the outer

mitochondrial membrane: mapping and identification of two new isoforms.

Genomics 20, 62-67.

Blachly-Dyson, E., Peng, S., Colombini, M., and Forte, M. (1990). Selectivity changes in site-directed mutants of the VDAC ion channel: Structural implications. *Science* 247, 1233-1236.

Blachly-Dyson, E., Peng, S. Z., Colombini, M., and Forte, M. (1989). Probing the structure of the mitochondrial channel, VDAC, by site-directed mutagenesis: A progress report. *J. Bioenerg. Biomembr.* 21, 471-483.

Blachly-Dyson, E., Zambronicz, E. B., Yu, W. H., Adams, V., McCabe, E. R., Adelman, J., Colombini, M., and Forte, M. (1993). Cloning and functional expression in yeast of two human isoforms of the outer mitochondrial membrane channel, the voltage-dependent anion channel. *J. Biol. Chem.* 268, 1835-1841.

Bollag, D. M., and Edelstein, S. J. (1991). "Protein Methods." Wiley-Liss Inc., New York.

Buettner, R., Papoutsoglou, G., Scemes, E., Spray, D. C., and Dermietzel, R. (2000). Evidence for secretory pathway localization of a voltage-dependent anion channel isoform. *Proc. Natl. Acad. Sci. U. S. A.* 97, 3201-3206.

Bullock, W. O., Fernandez, J. M., and Short, J. M. (1987). XL1-Blue: A high efficiency plasmid transforming recA *Escherichia coli* strain with beta-galactosidase selection. *BioTechniques* 5, 376.

Bureau, M. H., Khrestchatisky, M., Heeren, M. A., Zambrowicz, E. B., Kim, H., Grisar, T. M., Colombini, M., Tobin, A. J., and Olsen, R. W. (1992). Isolation and cloning

- of a voltage-dependent anion channel-like Mr 36,000 polypeptide from mammalian brain. *J. Biol. Chem.* 267, 8679-8684.
- Colombini, M. (1979). A candidate for the permeability pathway of the outer mitochondrial membrane. *Nature* 279, 643-645.
- Colombini, M., Blachly-Dyson, E., and Forte, M. (1996). VDAC, a channel in the outer mitochondrial membrane. *Ion Channels* 4, 169-202.
- Colombini, M., Yeung, C. L., Tung, J., and Konig, T. (1987). The mitochondrial outer membrane channel, VDAC, is regulated by a synthetic polyanion. *Biochim. Biophys. Acta* 905, 279-286.
- Cowan, S. W., Schirmer, T., Rummel, G., Steiert, M., Ghosh, R., Pauptit, R. A., Jansonius, J. N., and Rosenbusch, J. P. (1992). Crystal structures explain functional properties of two *E. coli* porins. *Nature* 358, 727-733.
- Crompton, M., Virji, S., and Ward, J. M. (1998). Cyclophilin-D binds strongly to complexes of the voltage-dependent anion channel and the adenine nucleotide translocase to form the permeability transition pore. *Eur. J. Biochem.* 258, 729-735.
- De Pinto, V., Prezioso, G., Thinnes, F., Link, T. A., and Palmieri, F. (1991). Peptide-specific antibodies and proteases as probes of the transmembrane topology of the bovine heart mitochondrial porin. *Biochemistry* 30, 10191-10200.
- Derrick, J. P., Urwin, R., Suker, J., Feaves, I. M., and Maiden, M. C. J. (1999). Structural and evolutionary inferences from molecular variation in *Neisseria* porins. *Inf. Imm.* 67, 2406-2413.

- Dolder, M., Zeth, K., Tittmann, P., Gross, H., Welte, W., and Wallimann, T. (1999). Crystallization of the human, mitochondrial voltage-dependent anion-selective channel in the presence of phospholipids. *J. Struct. Biol.* 127, 64-71.
- Elkeles, A., Devos, K. M., Graur, D., Zizi, M., and Breiman, A. (1995). Multiple cDNAs of wheat voltage-dependent anion channels (VDAC): isolation, differential expression, mapping and evolution. *Plant Mol. Biol.* 29, 109-124.
- Fischer, K., Weber, A., Brink, S., Arbinger, B., Schuenemann, D., Borchert, S., Heldt, H. W., Popp, B., Benz, R., Link, T. A., Ekerscorn, C., and Fluegge, U.-I. (1994). Porins from plants. Molecular cloning and functional characterization of two new members of the porin family. *J. Biol. Chem.* 269, 25754-25760.
- Forst, S., Waukau, J., Leisman, G., Exner, M., and Hancock, R. (1995). Functional and regulatory analysis of the OmpF-like porin, OpnP, of the symbiotic bacterium *Xenorhabdus nematophilus*. *Mol. Microbiol.* 18, 779-789.
- Forte, M., Guy, H. R., and Mannella, C. A. (1987). Molecular genetics of the VDAC ion channel: structural model and sequence analysis. *J. Bioenerg. Biomembr.* 19, 341-350.
- Garnier, J., Osguthorpe, D. J., and Robson, B. (1978). Analysis of the accuracy and implications of simple methods for predicting the secondary structure of globular proteins. *J. Mol. Biol.* 120, 97-120.
- Guibert, B., Dermietzel, R., and Siemen, D. (1998). Large conductance channel in plasma membranes of astrocytic cells is functionally related to mitochondrial VDAC-channels. *Int. J. Biochem. Cell Biol.* 30, 379-391.

- Ha, H., Hajek, P., Bedwell, D. M., and Burrows, P. D. (1993). A mitochondrial porin cDNA predicts the existence of multiple human porins. *J. Biol. Chem.* 268, 12143-12149.
- Hanahan, D. (1983). Studies on transformation of *Escherichia coli* with plasmids. *J. Mol. Biol.* 166, 557.
- Heins, L., Mentzel, H., Schmid, A., Benz, R., and Schmitz, U. K. (1994). Biochemical, molecular, and functional characterization of porin isoforms from potato mitochondria. *J. Biol. Chem.* 269, 26402-26410.
- Hodge, T., and Colombini, M. (1997). Regulation of metabolite flux through voltage-gating of VDAC channels. *J. Membr. Biol.* 157, 271-279.
- Huizing, M., Ruitenbeek, W., Thinnes, F. P., De Pinto, V., Wendel, U., Trijbels, F. J. M., Smit, L. M. E., Ter Laak, H. J., and Van Den Heuvel, L. P. (1996). Deficiency of the voltage-dependent anion channel: a novel cause of mitochondriopathy. *Pediatr. Res.* 39, 760-765.
- Jap, B. K., and Walian, P. J. (1996). Structure and functional mechanisms of porins. *Physiol. Rev.* 76, 1073-1088.
- Kayser, H., Kratzin, H. D., Thinnes, F. P., Gotz, H., Schmidt, W. E., Eckart, K., and Hilschmann, N. (1989). Identification of human porins. Characterization and primary structure of a 31-kDa porin from human B lymphocytes (Porin 31HL). *Biol. Chem. Hoppe-Seyler* 370, 1265-1278.
- Kleene, R., Pfanner, N., Pfaller, R., Link, T. A., Sebald, W., Neupert, W., and Tropschug, M. (1987). Mitochondrial porin of *Neurospora crassa*: cDNA cloning, *in vitro*

- expression and import into mitochondria. *EMBO J.* 6, 2627-2633.
- Koppel, D. A., Kinnally, K. W., Masters, P., Forte, M., Blachly-Dyson, E., and Mannella, C. A. (1998). Bacterial expression and characterization of the mitochondrial outer membrane channel. Effects of N-terminal modifications. *J. Biol. Chem.* 273, 13794-13800.
- Kunkel, T. A., Roberts, F. D., and Zakour, R. A. (1987). Rapid and efficient site-specific mutagenesis without phenotypic selection. *Meth. Enzymol.* 154, 367-382.
- Kyte, J., and Doolittle, R. F. (1982). A simple method for displaying the hydropathic character of a protein. *J. Mol. Biol.* 157, 105-132.
- Lee, A.-C., Xu, X., and Colombini, M. (1996). The role of pyridine dinucleotides in regulating the permeability of the mitochondrial outer membrane. *J. Biol. Chem.* 271, 26724-26731.
- Lou, K., Saint, N., Prilipov, A., Rummel, G., Benson, S. A., Rosenbusch, J. P., and Schirmer, T. (1996). Structural and functional characterization of OmpF porin mutants selected for larger pore size. I. Crystallographic analysis. *J. Biol. Chem.* 271, 20669-20675.
- Mannella, C. A. (1989). Structure of the mitochondrial outer membrane channel derived from electron microscopy of 2D crystals. *J. Bioenerg. Biomemb.* 21, 427-437.
- Mannella, C. A. (1997). On the structure and gating mechanism of the mitochondrial channel, VDAC. *J. Bioenerg. Biomemb.* 29, 525-531.
- Mannella, C. A., Forte, M., and Colombini, M. (1992). Toward the molecular structure of the mitochondrial channel, VDAC. *J. Bioenerg. Biomembr.* 24, 7-19.

- Mihara, K., and Sato, R. (1985). Molecular cloning and sequencing of cDNA for yeast porin, an outer mitochondrial membrane protein: a search for targeting signal in the primary structure. *EMBO J.* 4, 769-774.
- Moon, J. I., Jung, Y. W., Ko, B. H., De Pinto, V., Jin, I., and Moon, I. S. (1999). Presence of a voltage-dependent anion channel 1 in the rat postsynaptic density fraction. *Neuroreport.* 10, 443-447.
- Mutoh, N., Inokuchi, K., and Mizushima, S. (1982). Amino acid sequence of the signal peptide of OmpF, a major outer membrane protein of *Escherichia coli*. *FEBS Letters* 137, 171-174.
- Overbeeke, N., Bergmans, H., van Mansfeld, F., and Lgtenburg, B. (1983). Complete nucleotide sequence of phoE, the structural gene for the phosphate limitation inducible outer membrane pore protein of *Escherichia coli* K12. *J. Mol. Biol.* 163, 513-532.
- Park, K., Perczel, A., and Fasman, G. D. (1992). Differentiation between transmembrane helices and peripheral helices by the deconvolution of circular dichroism spectra of membrane proteins. *Prot. Sci.* 1, 1032-1049.
- Peng, S., Blachly-Dyson, E., Forte, M., and Colombini, M. (1992). Large scale rearrangement of protein domains is associated with voltage gating of the VDAC channel. *Biophys. J.* 62, 123-135.
- Perczel, A., Park, K., and Fasman, G. D. (1992). Analysis of the circular dichroism spectrum of proteins using the convex constraint algorithm: A practical guide. *Anal. Biochem.* 203, 83-93.

- Peter, M. E., Hall, C., Ruhlmann, A., Sancho, J., and Terhorst, C. (1992). The T-cell receptor ζ chain contains a GTP/GDP binding site. *EMBO J.* 11, 933-941.
- Phale, P. S., Philippsen, A., Kiefhaber, T., Koebnik, R., Phale, V. P., Schirmer, T., and Rosenbusch, J. P. (1998). Stability of trimeric OmpF porin: the contributions of the latching loop L2. *Biochemistry* 37, 15663-15670.
- Popp, B. (1996). . University of Wuerzburg, Wuerzburg, Germany.
- Popp, B., Court, D. A., Benz, R., Neupert, W., and Lill, R. (1996). The role of the N and C termini of recombinant *Neurospora* mitochondrial porin in channel formation and voltage-dependent gating. *J. Biol. Chem.* 271, 13593-13599.
- Popp, B., Gebauer, S., Fischer, K., Fluegge, U.-I., and Benz, R. (1997). Study of structure and function of recombinant pea root plastid porin by biophysical methods. *Biochemistry* 36, 2844-2852.
- Popp, B., Schmid, A., and Benz, R. (1995). Role of sterols in the functional reconstitution of water-soluble mitochondrial porins from different organisms. *Biochemistry* 34, 3352-3361.
- Rauch, G., and Moran, O. (1994). On the structure of mitochondrial porins and its homologies with bacterial porin. *Biochem. Biophys. Res. Commun.* 200, 908-915.
- Reymann, S., Haase, W., Krick, W., Burckhardt, G., and Thinner, F. P. (1998). Endosomes: another extra-mitochondrial location of type-1 porin/voltage-dependent anion-selective channels. *Pflügers* 436, 478-480.
- Roos, N., Benz, R., and Brdiczka, D. (1982). Identification and characterization of the pore-forming protein in the outer membrane of rat liver mitochondria. *Biochim.*

Biophys. Acta 686, 204-214.

Rostovtseva, T., and Colombini, M. (1997). VDAC channels mediate and gate the flow of ATP: implications for the regulation of mitochondrial function. *Biophys. J.* 72, 1954-1962.

Rudel, T., Schmid, A., Benz, R., Kolb, H.-A., Land, F., and Meyer, T. F. (1996). Modulation of *Neisseria* porin (PorB) by cytosolic ATP/GTP of target cells: parallels between pathogen accommodation and mitochondrial endosymbiosis. *Cell* 85, 391-402.

Saint, N., Lou, K., Widmer, C., Luckey, M., Schirmer, T., and Rosenbusch, J. P. (1996). Structural and functional characterization of OmpF porin mutants selected for larger pore size. *J. Biol. Chem.* 271, 20676-20680.

Samartzidou, H., and Delcour, A. H. (1998). *E. coli* PhoE porin has an opposite voltage-dependence to the homologous OmpF. *EMBO J.* 17, 93-100.

Samartzidou, H., and Delcour, A. H. (1999). Distinct sensitivities of OmpF and PhoE porins to charged modulators. *FEBS Lett.* 444, 65-70.

Sambrook, J., Fritsch, E. F., and Maniatis, T. (1989). "Molecular cloning. A laboratory manual." Cold Spring Harbor Press, Cold Spring Harbor, N.Y.

Sampson, M. J., Lovell, R. S., and Craigen, W. J. (1996a). Isolation, characterization, and mapping of two mouse mitochondrial voltage-dependent anion channel isoforms. *Genomics* 33, 283-288.

Sampson, M. J., Lovell, R. S., Davison, D. B., and Craigen, W. J. (1996b). A novel mouse mitochondrial voltage-dependent anion channel gene localizes to chromosome 8.

Genomics 36, 192-196.

Schein, S. J., Colombini, M., and Finkelstein, A. (1976). Reconstitution in planar lipid bilayers of a voltage-dependent anion-selective channel obtained from *Paramecium* mitochondria. *J. Memb. Biol.* 30, 99-120.

Schirmer, T., and Phale, P. S. (1999). Brownian dynamics simulation of ion flow through porin channels. *J. Mol. Biol.* 294, 1159-1167.

Seshardi, K., Garemyr, R., Wallin, E., Von Heijne, G., and Elofsson, A. (1998). Architecture of β -barrel membrane proteins: Analysis of trimeric porins. *Prot. Sci.* 7, 2026-2032.

Shafir, I., Feng, W., and Shoshan-Barmataz, V. (1998). Voltage-dependent anion channel proteins in synaptosomes of the torpedo electric organ: immunolocalization, purification, and characterization. *J. Bioenerg. Biomembr.* 30, 499-510.

Shao, L., Kinnally, K. W., and Mannella, C. A. (1996). Circular dichroism studies of the mitochondrial channel, VDAC, from *Neurospora crassa*. *Biophys. J.* 71, 778-786.

Shimizu, S., Narita, M., and Tsujimoto, Y. (1999). Bcl-2 family proteins regulate the release of apoptogenic cytochrome c by the mitochondrial channel VDAC. *Nature* 399, 483-487.

Shoshan-Barmatz, V., Hadad, N., Feng, W., Shafir, I., Orr, I., Varsanyi, M., and Heilmeyer, L. M. (1996). VDAC/porin is present in sarcoplasmic reticulum from skeletal muscle. *FEBS Lett.* 386, 205-210.

Song, J., and Colombini, M. (1996). Indications of a common folding pattern for VDAC channels from all sources. *J. Bioenerg. Biomembr.* 28, 153-61.

- Song, J., Midson, C., Blachly-Dyson, E., Forte, M., and Colombini, M. (1998a). The sensor regions of VDAC are translocated from within the membrane to the surface during the gating process. *Biophys. J.* 74, 2962-2944.
- Song, J., Midson, C., Blachly-Dyson, E., Forte, M., and Colombini, M. (1998b). The topology of VDAC as probed by biotin modification. *J. Biol. Chem.* 273, 24406-24413.
- Stanley, S., Dias, J. A., D'Arcangelis, D., and Mannella, C. A. (1995). Peptide-specific antibodies as probes of the topography of the voltage-gated channel in the mitochondrial outer membrane of *Neurospora crassa*. *J. Biol. Chem.* 270, 16694-16700.
- Steinacker, P., Awni, L. A., Becker, S., Cole, T., Reymann, S., Hesse, D., Kratzin, H. D., Morris-Wortmann, C., Schwarzer, C., Thinnies, F. P., and Hilschmann, N. (2000). The plasma membrane of *Xenopus laevis* oocytes contains voltage-dependent anion-selective porin channels. *Int. J. Biochem. Cell. Biol.* 32, 225-234.
- Thomas, L., Blachly-Dyson, E., Colombini, M., and Forte, M. (1993). Mapping of residues forming the voltage sensor of the voltage-dependent anion-selective channel. *Proc. Natl. Acad. Sci. U. S. A.* 90, 5446-5449.
- Thompson, J. D., Higgins, D. G., and Gibson, T. (1994). CLUSTAL W: improving the sensitivity of progressive multiple sequence alignment through sequence weighting, position-specific gap penalties and weight matrix choice. *Nucl. Acids Res.* 22, 4673-4680.
- Troll, H., Malchow, D., Muller-Taubenberger, A., Humbel, B., Lottspeich, F., Ecker, M.,

- Gerisch, G., Schmid, A., and Benz, R. (1992). Purification, functional characterization and cDNA sequencing of mitochondrial porin from *Dictyostelium Discoideum*. *J. Biol. Chem.* 267, 21072-21079.
- Villarejo, M. R., and Zabin, I. (1974). β -Galactosidase from termination and deletion mutant strains. *J. Bacteriol.* 120, 466-474.
- Zalman, L. S., Nikaido, H., and Kagawa, Y. (1980). Mitochondrial outer membrane contains a protein producing nonspecific diffusion channels. *J. Biol. Chem.* 255, 1771-1774.
- Zizi, M., Byrd, C., Boxus, R., and Colombini, M. (1998). The voltage-gating process of the voltage-dependent anion channel is sensitive to ion flow. *Biophys. J.* 75, 704-713.